Design Principles and Performance Metrics for Magnetic Refrigerators Operating Near Room Temperature

by

Daniel Sean Robert Arnold

A Dissertation Submitted in Partial Fulfillment
of the Requirements for the Degree of

MASTER OF APPLIED SCIENCE

in the Department of Mechanical Engineering

Supervisory Committee

Design Principles and Performance Metrics for Magnetic Refrigerators Operating Near Room Temperature

by

Daniel Sean Robert Arnold
Bachelor of Engineering, University of Victoria, 2009

Supervisory Committee

Dr. Andrew Rowe, (Department of Mechanical Engineering)
Supervisor

Dr. Peter Wild, (Department of Mechanical Engineering)
Departmental Member

Abstract

Supervisory Committee
Dr. Andrew Rowe, (Department of Mechanical Engineering)
Supervisor
Dr. Peter Wild, (Department of Mechanical Engineering)
Departmental Member

In the past decade, active magnetic regenerative (AMR) refrigeration technology has progressed towards commercial application. The number of prototype systems and test apparatuses has steadily increased thanks to the worldwide research efforts. Due to the extensive variety of possible implementations of AMR, design methods are not well established. This thesis proposes a framework for approaching AMR device design.

The University of Victoria now has three functional AMR Refrigerators. The newest system constructed in 2012 operates near-room-temperature and is intended primarily as a modular test apparatus with a broad range of control parameters and operating conditions. The design objectives, considerations and analysis are presented.

Extensive data has been collected using the machines at the University of Victoria. Performance metrics are used to compare the devices. A semi-analytical relationship is developed that can be used as an effective modelling tool during the design process.

Table of Contents

List of Tables

List of Figures

Nomenclature

Acronyms

AMR	Active Magnetic Regenerator (or Regenerative)
COP	Coefficient of Performance
FOM	Figure of Merit
HTF	Heat Transfer Fluid
MCM	Magnetocaloric Material
MCE	Magnetocaloric Effect (adiabatic temperature change)
MR	Magnetic Refrigeration
PMTA-1	Permanent Magnet Test Apparatus, Generation I
PMTA-2	Permanent Magnet Test Apparatus, Generation II
SCMTA	Superconducting Magnet Test Apparatus
UVic	University of Victoria

Symbols

a, b, c, d	Discrete state points	-
a	Magnet capacity factor	-
A	Area (cross-sectional or surface)	m^2
b	Number of high field regions	-
B	Magnetic flux density	T
c	Specific heat capacity	$J\ kg^{-1}\ K^{-1}$
C	Heat capacity	$J\ K^{-1}$
d	Number of regenerators per field region	-
D	Diameter	m
D	Device configuration designator	-
Ex	Exergy	J
f	Machine frequency	s^{-1}
F	Friction factor	-
G	Gibbs free energy	J
h	Specific enthalpy	$J\ kg^{-1}$
$\bar{h}$	Convection coefficient	$W\ m^{-2}\ K^{-1}$
H	Enthalpy	J
H	Magnetic field strength	$A\ m^{-1}$
L	Length	m
m	Mass	kg
$\bar{m}$	Mass magnetization	$A\ m^2\ kg^{-1}$
M	Magnetization	$A\ m^{-1}$
P	Pressure	$N\ m^{-2}$
Q	Heat transfer	J
r	Number of discrete regenerators	-

R	Thermal mass ratio	-
s	Specific entropy	J kg^{-1} K^{-1}
S	Entropy,	J K^{-1}
t	Time	s
T	Temperature	K
u	Specific internal energy	J kg^{-1}
U	Internal energy	J
v	Velocity	m s^{-1}
V	Volume	m^3
W	Work	J
x	Spatial coordinate	m

Greek

α	Porosity	-
κ	Non-dimensional conductance	-
μ	Viscosity	Pa s
$\bar{\mu}$	Specific exergetic cooling power	W T^{-1} m^{-1}
μ_0	Magnetic permeability of free space	T A^{-1} m
σ	effective conductance loss coefficient	W K^{-1}
ρ	Density	kg m^{-3}
τ	Period	s
Δ	Total change (low to high magnetic field)	-
θ	Angle	Degrees
$\dot{\varphi}$	Capacity rate	s^{-1}
Φ	Utilization	-
$\bar{\Phi}$	Reference utilization	-

Subscripts

0	Free space	-
a	Applied	-
ad	Adiabatic	-
b	Blow	-
B	Magnetic flux density	-
c	Cycle	-
$config$	Configuration	-
$curie$	Curie (temperature)	-
$cycle$	Cycle	-
C	Cold, Cooling	-
$device$	Device	-
$eddy$	Eddy Current	-
f	Fluid	-
g	Bearing support structure	-

h	High (magnetic field)	-
h	Hydraulic (diameter)	-
H	Hot	-
irr	Irreversible	-
L	Leak (regenerator heat leak)	-
l	Low (magnetic field)	-
$mech$	Mechanical	-
M	Magnetic	-
MCM	Magnetocaloric Material	-
net	Net	-
p	Parasitic (environmental heat leak)	-
p	Particle (diameter)	-
p	Pore (velocity)	-
P	Pump (work)	-
PM	Permanent Magnet	-
Q	Cooling Power	-
r	Regenerator	-
rev	Reversible	-
$S-A$	Semi-Analytical	-
s	Solid	-
$span$	Span	-
w	Wetted	-
∞	Ambient or Environment	-

Superscripts

$\bar{\square}$	Mean, Cycle Averaged	-
$\hat{\square}$	Non-dimensional	-
$\dot{\square}$	Per unit time	-
$\square'$	Per unit length	-

Acknowledgments

I would like to chiefly acknowledge the support and guidance provided by my supervisor, Andrew Rowe. I also wish to acknowledge my valued colleagues involved in magnetic refrigeration research: Armando Tura, Thomas Burdyny, Sandro Schopfer, Alexander Ruebsaat-Trott, Oliver Campbell, Paulo Trevizoli, Kasper Nielsen, and Rodney Katz.

The financial support provided by the Natural Science and Engineering Research Council of Canada is also greatly appreciated.

Dedication

This thesis is dedicated to my family. This work would never have been realized without the love and support of my wife, Jennie, and the inspiration of my children, Declan and Alena. I also wish to recognize my parents, Lynn and Paul, and my brother, Patrick, for their support.

Chapter 1: Introduction

1.1. Motivation

As awareness has grown regarding environmental impact due to energy harvesting and consumption, efforts to deliver services with greater energy efficiency have increased. These efforts extend to transportation, manufacturing, agriculture, heating and cooling. Refrigeration, from residential cooling to liquefaction of gases, represents a significant fraction of the total world energy demand. The conventional approach of compressing a vapour has historically dominated in all applications. Refrigerators using this approach are inexpensive to construct; unfortunately, the process efficiency is impacted due to the commonly used isenthalpic expansion method which is inherently irreversible. Vapour compression devices also typically rely on refrigerants that are known to deplete the ozone layer, are greenhouse gases or may be toxic and flammable. To provide cooling in a more environmentally and energy conscience fashion, alternative refrigeration technologies are being explored.

In the past two decades, magnetic refrigeration technology based upon the active magnetic regenerative (AMR) cycle has progressed significantly. The AMR cycle has the theoretical potential to achieve efficiencies comparable to that of a Carnot cycle due to the reversible magnetic work mode. Implementation of magnetic refrigeration is feasible; however, the performance and cost targets have not yet been met to make this technology viable in the marketplace. Further research and development is still required.

Originally, AMR based refrigeration was investigated for cryogenic applications where small efficiency improvements could translate into significant energy savings. More recently, magnetic refrigeration has been studied for use in near-room-temperature applications. Considerable advancements have been made in this area including prototype development and

experimental analysis [1], material characterization and synthesis, and numerical simulations [2]. As more prototype machines are constructed, it becomes increasingly difficult to categorize and compare the different systems due to the extensive variety of implementation method and scale. Likewise, the numerical simulations that exist to predict AMR cycle performance vary in terms of methodology and complexity. The models are often computationally intensive making it difficult to cover the operational space in reasonable time. In the case of conventional vapour-compression type systems, standards have been developed that dictate principles and categories of design, methods of scaling systems for given applications as well as metrics for performance assessment. Because magnetic refrigeration is a young technology that has not yet achieved commercialization, equivalent standards, methods and metrics have not yet been defined and accepted.

1.2. AMR Fundamentals

Magnetic refrigeration relies on certain fundamental effects: the response of a solid material to an applied magnetic field, the thermal interactions between this solid material constructed as a porous media and an entrained fluid, as well as how these are employed in a thermodynamic cycle to produce cooling. These concepts will be introduced in this section.

1.2.1. Magnetocaloric Refrigerants

Magnetocaloric materials (MCM) exhibit a reversible thermal response when exposed to variations in applied magnetic field intensity. This is referred to as the magnetocaloric effect (MCE) which was first observed by Weiss and Picard in 1917 [3]. The application of a magnetic field causes the internal magnetic dipoles of an MCM to align which results in a reduction in magnetic entropy. To balance the second law for the solid under adiabatic conditions, there is a subsequent increase in lattice entropy or temperature. In other words, forcing a change in the

magnetic state of the solid is balanced by a change in the thermal state. This is analogous to the temperature increase seen when adiabatically compressing a vapour. It is this dependence between magnetization and temperature that allow MCMs to be used in a thermodynamic process to transport heat. The compression and expansion methods used in conventional vapour-compression cycles exhibit irreversibilities. In particular, Joule-Thompson (isenthalpic) expansion from high to low pressure is mechanically convenient but is inherently irreversible. A significant appeal of MCMs as a solid refrigerant is that the magnetic-temperature response, under adiabatic conditions and neglecting mechanical losses, can be reversible in application.

The MCE of most commonly observed materials display strong dependence on initial temperature. The peak adiabatic temperature change of a material typically occurs at one temperature where the substance undergoes a magnetic phase transition. This concept will be expanded upon in the proceeding chapter. The peak adiabatic temperature change for most of these common materials due to the applied magnetic field is on the order of 2-3 Kelvin per Tesla; therefore, a simple cycle is limited to approximately 10 degrees of span between two thermal reservoirs depending on the applied magnetic field [4]. Because of the relatively small temperature change of MCMs, another thermal mechanism must be employed to achieve the higher temperature spans required for typical cooling applications. In an AMR, the MCMs are constructed as porous media and function as regenerators. This technique allows for higher temperature differences between a cold zone and a heat rejection reservoir to be realized.

1.2.2. Regeneration

Traditional passive regenerators are a solid thermal mass constructed as porous media with a high surface area to volume ratio. A heat transfer fluid (HTF) oscillates through the regenerator matrix where it either dissipates or absorbs heat to or from the solid respectively. In

this way, an ideal regenerator acts as a perfect thermal resistor thereby isolating two temperature reservoirs. Passive regeneration is the process of transferring thermal energy between an oscillating fluid and a solid porous media to maintain a temperature differential between two fluid reservoirs across the matrix. An example of a temperature profile across a passive regenerator matrix is displayed in Figure 1. This cross-sectional view is oriented perpendicular to the direction of flow along x. The figure displays variation of the temperature profile according to the regenerator effectiveness. An ineffective regenerator does not fully isolate the two reservoirs resulting in heat flux. This concept will be elaborated upon later.

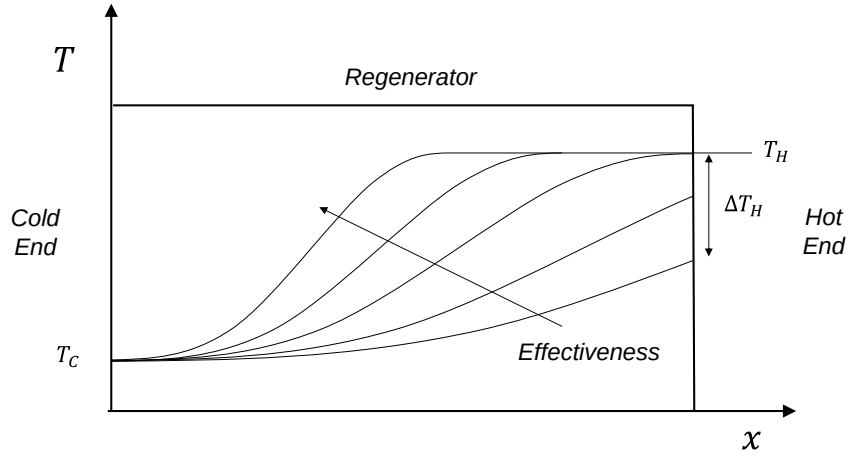

Figure 1: Example of various temperature profiles across a regenerator during a cold blow. The variability is dependent on the regenerator effectiveness which goes up according to the arrow.

Regenerators are widely used in other applications outside of AMR, particularly in cryogenic cooling machines such as pulse tubes or Gifford-McMahon cryo-coolers. Knowledge regarding regenerator construction and characterization is extensive pertaining to these applications. While not directly equivalent, this knowledge base is transferrable to AMR development.

When MCMs are constructed as regenerators they are referred to as active magnetic regenerators. They are active because the magnetic response of the material perturbs the

temperatures within the regenerator and consequently drives heat transfer. The active regenerator functions to both maintain a temperature span between two thermal reservoirs and pump heat from one reservoir to the other. This is the basis of the AMR cycle.

1.2.3. AMR Cycle

The active magnetic regenerative (AMR) cycle employs MCMs as the solid working refrigerant. One or more materials are used to construct an active magnetic regenerator. The active regenerator is cycled between high and low magnetization states. A HTF is then displaced through the active magnetic regenerator in a specified phase relative to the magnetization cycle to transport heat from a cold zone to a heat rejection reservoir. These two sets of fundamental physics, refrigerant magnetization and regeneration, must cooperate to produce an effective AMR cycle.

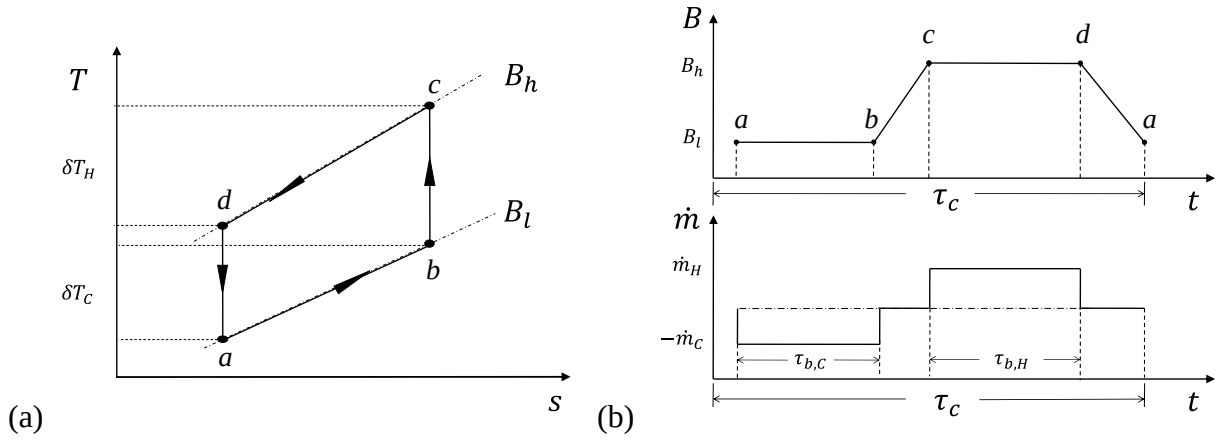

Figure 2: (a) *T-s* diagram of AMR cycle at an arbitrary location in the regenerator. (b) AMR cycle magnetic field and relative HTF timing waveforms [5].

The ideal magnetization and regeneration process of the AMR cycle for an arbitrary location within the regenerator is described by the *T-s* diagram in Figure 2(a) and can be discussed in terms of four distinct state points: (*a*→*b*) isofield heat absorption from the HTF, (*b*→*c*) adiabatic, isentropic magnetization of MCM, (*c*→*d*) isofield heat rejection to the HTF,

($d \rightarrow a$) adiabatic, isentropic demagnetization of MCM. The enclosed area is proportional to the local net magnetic work per unit length [5]. The magnetic field cycle and HTF flow cycle must occur at the appropriate times relative to each other as presented in Figure 2(b). The state points shown in 2(b) correspond to those in 2(a). The flow waveform shows the fluid flow as constant over the *blow period*. This exemplary flow waveform conveys that the cold and hot blow occur in opposite direction and that there may be a dwell period such that the sum of the blow periods, $\tau_{b,C} + \tau_{b,H}$, is less than the cycle period, τ_c.

To better comprehend how the AMR cycle behaves, Figure 3 illustrates the four processes of the AMR cycle as discussed above compared to the analogous processes of a traditional vapour refrigeration cycle. The magnetization of the solid refrigerant is comparable to the compression of the vapour refrigerant. The most significant different to AMR is that the vapour refrigerant employed in conventional cycles is also the heat transfer fluid.

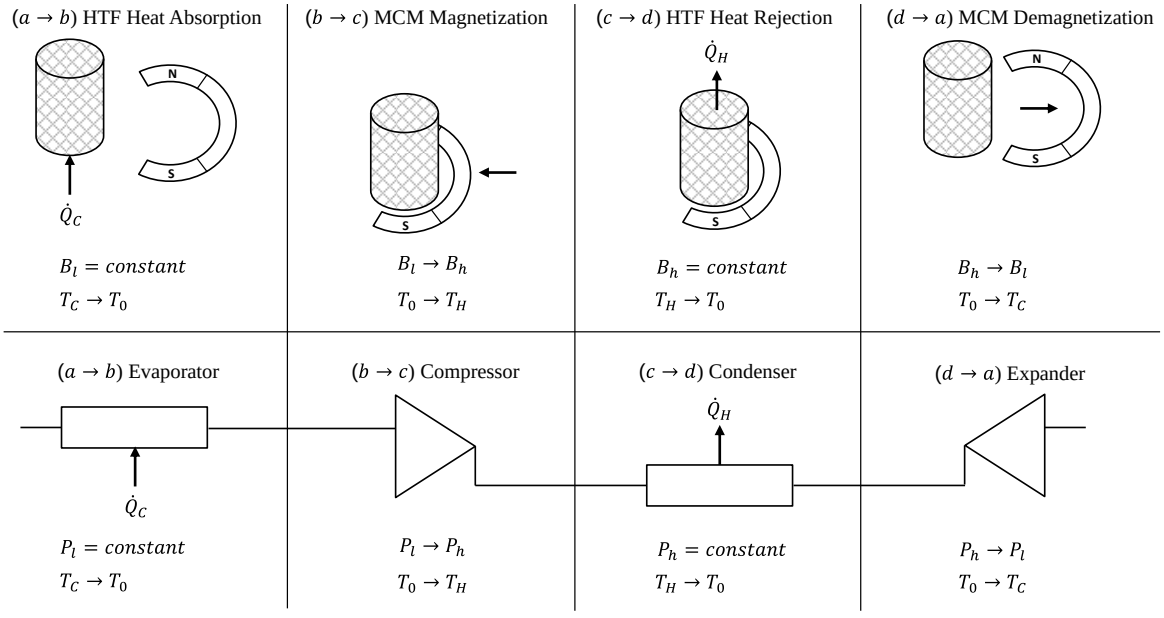

Figure 3: Simplified representations of an AMR refrigerator compared to a conventional refrigerator in terms of the four cycle state points.

1.3. Magnetic Refrigeration Devices

There are many possible configurations and construction styles of AMR devices. A variety of machines have been built operating in differing ranges of temperature span and cooling power [1] [6]. Differences in design are determined by numerous factors:

1. *magnetocaloric material*

Magnetocaloric refrigerants are broadly classed as either first order or second order materials. This refers to the nature of the magnetic phase transition and the subsequent behaviour of the magnetic entropy and heat capacity properties as a function of temperatures and magnetic field [7]. This concept will be elaborated upon in subsequent chapters. The MCE and heat capacity of a material are of primary interest. Density and thermal conductivity are also relevant to the AMR cycle. Classifying the characteristics and functional behaviour of MCMs for use in AMR cycles is an area of ongoing research. The mechanical properties of the materials, such as ductility, are relevant to the workability of these materials as regenerator structures.

2. *morphology of the regenerator*

Morphology refers to the physical geometry of the porous matrix. Various geometries have historically been used in applications outside of magnetic refrigeration: crushed irregular particles, spherical particles, parallel platelets, stacked wire mesh, stacked parallel tubes and channelled microstructures. Sample images of spheres, woven mesh and a micro-channel structure are presented in Figure 4.

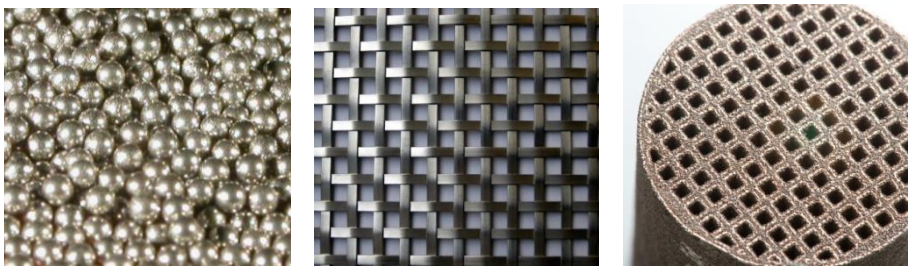

Figure 4: Examples of possible regenerator geometries.

Depending on the MCM, some of these traditional geometries may be unavailable due to the limits of the material and the manufacturing techniques that are available.

3. *heat transfer fluid*

HTFs used in AMRs can be broadly grouped into two categories: high thermal density liquids or low thermal density gases. Liquid HTFs such as water are predominately used in near-room-temperature AMR devices; however, gases such as air and helium are also used. The successful use of these benign HTFs highlights the environmental appeal of AMR technology. The role of the HTF is to transport energy from one temperature reservoir to another while requiring minimal pumping work. Important properties include density, viscosity, heat capacity and thermal conductivity.

4. *magnetic field generator*

The magnetic field generator can be broadly grouped into two categories: superconducting electro-magnet and permanent magnets.

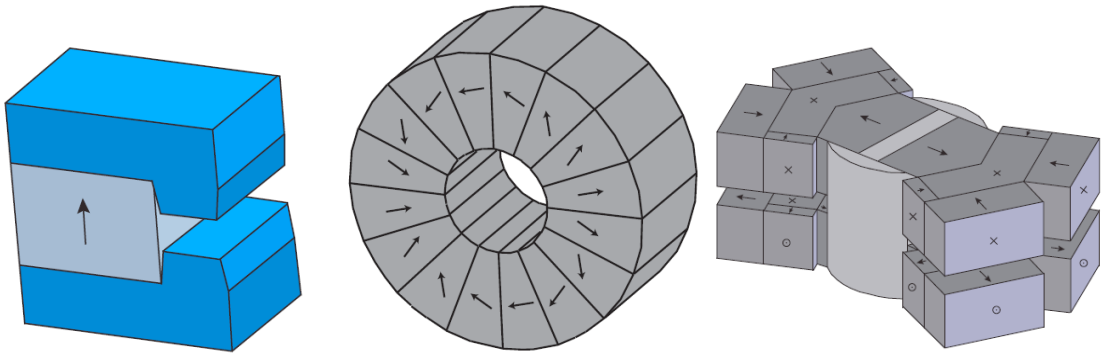

Figure 5: Examples of different magnetic field generator types [8].

Permanent magnets are most commonly used in near-room-temperature AMR devices [8]. The classification of permanent magnets can be expanded further into simple dipole structures, Halbach type arrangements which can either be single-pole, multi-pole or nested, as well as complex multi-pole arrangements. The magnetic field can either be oriented axially or

transversely relative to the fluid flow axis of the regenerator. A simple dipole, Halbach array and complex structure are presented in Figure 5.

5. relative number of regenerators and magnetic field regions

Devices can be constructed with multiple regenerators and multiple high magnetic field regions. The relative number of each affects the mechanical implementation, cooling potential and cost. It is valuable to know how effectively the magnetic field generator and refrigerate are employed, recognizing that these elements typically dominate the capital cost of a magnetic refrigerator [9].

6. method of displacing the heat transfer fluid

When considering the AMR cycle, the HTF must always oscillate through the regenerator in a relative phase to the magnetic oscillations. When considering the device, the HTF can be displaced through the external system in either a continuous or modulating fashion [10]. In the modulating case, the flow of the HTF throughout the external flow systems is coupled to the oscillation through the regenerator. This is mechanically convenient because the regenerator can be connected directly to a simple displacer mechanism such as a piston-cylinder; however, there are undesirable consequences including stagnant fluid volumes and reduced heat exchanger effectiveness. These effects will be elaborated upon later. In the case of continuous displacement, the flow of the HTF travels uni-directionally through the external flow circuit and then is converted to oscillating flow through the regenerator by a valve mechanism. A common uni-directional pump can be used to drive the fluid flow.

7. relative mechanical motion of the regenerator and field generator

Because the active regenerator must change magnetic state, some relative motion between the regenerator and magnetic field generator is required. The mechanical motion of

AMR devices is divided into rotary and reciprocating categories [1]. Rotary systems maintain constant rotational movement of either the magnets or regenerators with respect to the other about a fixed axis. For reciprocating systems, either the magnets or regenerators move over finite distance with respect to the other along a fixed axis.

1.4. Objectives

The University of Victoria (UVic) engages of all facets of magnetic refrigeration research and three functional AMR device currently exist at UVic. The construction of the latest machine was completed in September 2012. This system operates near-room-temperature and is intended primarily as a modular test apparatus with a broad range of control parameters and operating conditions. Extensive experimental data was collected for a range of materials and matrix geometries using the two previously existing machines. This experience and knowledge guided the design of the newest device.

Until recently, the design of AMR devices has been initiated with modest guidance from previous studies because few devices in the literature have produced a useful range of performance data. In many cases, each laboratory made design decisions based upon their own intuition or on design calculations that may not have been validated. The fact that numerous device designs have been reported, but only a fraction produce results that improve on previous data, indicates the need for a defined framework for approaching device design that has been validated through actual device performance data. Further, the complexity and limited accuracy of many AMR models highlights a need for simpler analytic approaches which can capture the impacts of the main design parameters with reasonable accuracy.

The purpose of this thesis is to develop a framework for AMR device design. This objective is met through the following contributions:

- define analytic expressions that describe the energy transfer mechanisms of an AMR refrigerator as a function of the dominant system parameters
- identify and characterize the primary elements and the design principles needed to develop an effective AMR refrigerator
- identify metrics for assessing and ranking the performance of an arbitrary AMR refrigerator
- discuss the development of a real AMR machine in context of the proposed design framework
- experimentally validate the analytic approach and the design framework using data collected using the devices and conditions available at UVic

Chapter 2 presents a comprehensive summary of the governing theory of MCMs and the AMR cycle. Simplified analytical expressions for magnetic work and cooling potential of the ideal AMR cycle are defined at the end of Chapter 2. The fundamental theory in the first half of the chapter is required to illustrate how the analytical expressions are arrived upon and also serves as a concise reference. Chapter 3 introduces the proposed framework for approaching device design in terms of an iterative process methodology. The energy transport behaviour and the primary operational parameters of a real AMR machine are outlined. Chapter 3 also presents a collection of metrics that can be used to assess device operational performance. Chapter 4 presents and classifies the machines available at UVic for experimentation. The development of the newest machine is discussed in context of the framework developed in Chapter 3. Chapter 5 presents experimental findings obtained from the devices available at UVic. In Chapter 6, the experimental results are analyzed and performance rankings are found. Based on the analytical expressions defined in Chapter 2, a semi-analytical expression for cooling power is validated.

Chapter 7 contains a final discussion regarding the investigation and presents conclusions and recommendations.

Chapter 2: Magnetic Refrigeration Theory

This chapter presents the fundamental theory relevant to magnetic refrigeration. The characteristics of magnetocaloric materials and their behaviour as refrigerants are presented. The relevant features of passive regenerators are discussed. A classical transient two-phase analysis of active regenerators is also presented. The idealized AMR cycle is examined. A method to define the temperature profile within the regenerator is included. Simplified analytical expressions for describing the energy transfer over the cycle are defined. With these expressions, the cycle-averaged cooling power and magnetic work consumption can be found by a direct calculation which is desirable for the design process.

2.1. Magnetocaloric Materials

The magnetic state of a solid is defined by its magnetization, M. Assuming a simple magnetic material where the only work mode is magnetic, the magnetization is a function of local magnetic field, H, and temperature, T. The reversible magnetic work, $W_{M,rev}$, required to change the magnetic state of the MCM is defined similarly to the reversible work required to change the volume of a simple compressible system, $W_{V,rev}$. Note the applied magnetic flux density, B, is related to the applied magnetic field, H_a, by the permeability of free space, μ_0, by the conventional relationship to $B = \mu_0 \mathrm{H}_a$. Demagnetization effects are ignored.

$$\delta W_{M,rev} = -BVdM \tag{1}$$

$$\delta W_{V,rev} = PdV \tag{2}$$

where magnet work done by the material is assumed positive and over the total volume [11]. When considering state changes in a magnetic solid material, both thermal and magnetic

components must be accounted for. The first law for a magnetic solid can be written for infinitesimal changes:

$$dU = \delta Q_{M,rev} - \delta W_{M,rev} \tag{3}$$

$$dU = TdS + BVdM \tag{4}$$

Likewise, the variation in magnetic enthalpy can be written:

$$dH = TdS - VMdB \tag{5}$$

And finally, the Gibbs free energy:

$$dG = -SdT - VMdB \tag{6}$$

From the Gibbs expression, a Maxwell's relation is found:

$$\left.\frac{\partial S}{\partial B}\right|_T = V \left.\frac{\partial M}{\partial T}\right|_B \tag{7}$$

The total entropy change for a simple magnetic solid is a sum of thermal and magnetic components. This is the essence of the MCE. The total entropy variation due to changes in temperature and magnetic flux is:

$$dS(T,B) = \left.\frac{\partial S}{\partial T}\right|_B dT + \left.\frac{\partial S}{\partial B}\right|_T dB \tag{8}$$

The isothermal magnetic components can be found from the Maxwell relation. The isofield thermal component can be found based on the heat capacity definition:

$$C_B(T,B) = mc_B(T,B) = T\left.\frac{\partial S}{\partial T}\right|_B \tag{9}$$

It is important to note that specific heat capacity is a function of temperature and the given constant magnetic flux. The total entropy variation can now be written as:

$$dS(T,B) = \frac{mc_B}{T}dT + V\left.\frac{\partial M}{\partial T}\right|_B dB \tag{10}$$

The original internal energy balance of equation (3) can now be expanded to include both entropy contributions:

$$dU = mc_B dT + TV\frac{\partial M}{\partial T}\Big|_B dB + BVdM \tag{11}$$

Enthalpy and Gibbs free energy can also be rewritten accordingly.

2.1.1. Adiabatic Temperature Change

The MCE can be defined as the temperature change of the MCM under isentropic conditions for a specified change in magnetic field at a specified initial temperature. Considering the adiabatic, reversible case where total entropy is conserved, the definition of the adiabatic temperature change, ΔT_{ad}, can be found from equation (10):

$$0 = dS(T, B) \tag{12}$$

$$\frac{mc_B}{T}dT = -V\frac{\partial M}{\partial T}\Big|_B dB \tag{13}$$

$$dT_{ad} = -\frac{TV}{mc_B}\frac{\partial M}{\partial T}\Big|_B dB \tag{14}$$

$$\Delta T_{ad} = -\int_{B_l}^{B_h}\frac{TV}{mc_B}\frac{\partial M}{\partial T}\Big|_B dB \tag{15}$$

A comprehensive measurement of MCMs is by the specific heat capacity, $c_B(T, B)$, moving from low to high temperatures at a constant magnetic field [7] [12]. Equation (9) can then be integrated to give the thermal entropy of the solid for a given magnetic field. Providing total entropy conservation is upheld, the magnetic entropy change is thereby known. If data is collected over a range of isofield conditions, then the adiabatic temperature change going from low to high flux $(B_l \rightarrow B_h)$ can be calculated from these measurements. This data is an essential resource for predicting the behaviour of MCMs when used as refrigerants in AMR cycles.

2.1.2. Curie Temperature

An important characteristic of MCMs is the Curie temperature. It is at this temperature where a simple magnetocaloric material undergoes a magnetic phase transition in the absence of an applied field. Often, this presents as a shift from a paramagnetic state ($T > T_{curie}$) to ferromagnetic behaviour ($T < T_{curie}$). The Curie temperature is a unique value for a given material. The maximum adiabatic temperature change is observed near the Curie temperature. This is due to the fact that the variation in magnetization with temperature is maximum at this transitional point. Generally, MCM phase transitions can be categorized into first-order and second-order behaviour. First-order materials display a sudden narrow spike in both ΔT_{ad} and c_B around T_{curie} whereas second-order materials display a broader, more gradual variation in ΔT_{ad} with temperature and a nearly constant value of c_B. Typically first-order materials achieve a greater peak value in magnetic entropy change than second-order materials for the same magnetic field change. Many of the better-known magnetocaloric materials are rare-earth alloys which display second-order behaviour.

2.1.3. Hysteresis

Due to recent concerns over supply and cost, attention has shifted away from rare-earth based second-order materials and focused on newly emerging alloys with tuneable first-order behaviour. Experimental investigation of different MCMs has shown that some second-order materials come very close to achieving the desired reversible thermomagnetic response while most first-order materials display history dependence [13]. History dependence in a thermodynamic process is referred to as hysteresis. To elaborate, any change is thermomagnetic state is dependent on the previous state or phase. This impacts the measurement of specific heat capacity and adiabatic temperature change. For example, measurements taken $T_l \rightarrow T_h$ or

$B_l \rightarrow B_h$ may not be the same as $T_h \rightarrow T_l$ or $B_h \rightarrow B_l$. Magnetic hysteresis has been experimentally observed as magnetization behaviour depending on previous magnetization state, direction of magnetization (increasing or decreasing) and rate of magnetization. This behaviour is sometimes referred to as magnetic memory or magnetic inertia and can be considered as a resistance to change in magnetization state. Considering a MCM, the temperature response is directly impacted by this effect. The resistance to changing magnetic state can be considered as an entropy generation mechanism which consequently would lead to some energy loss over a magnetic cycle. For the purposes of this investigation, these effects will only be discussed superficially.

2.2. Passive Regenerators

Passive regenerators store thermal energy with no internal work modes present in the material. They are assessed by their hydraulic properties which are chiefly characterized by the pressure drop across the matrix and the subsequent pump work requirement as well as their thermal properties which include the conductive heat transfer within the solid matrix, the convective heat transfer between solid and fluid, and any dispersive or dissipative effects.

2.2.1. Flow Characteristics

The flow through a regenerator is dependent on the structure of the matrix. An important parameter describing a regenerator matrix is porosity. The porosity is the percentage of void space compared to the regenerator housing volume and can be determined by:

$$\alpha = 1 - \frac{V_s}{V_r} \tag{16}$$

where V_s is the volume of the solid refrigerant and V_r is the total volume of the regenerator housing [14]. The hydraulic diameter of the system is defined by the ratio of flow area and

wetted perimeter. It can be calculated as the volume of entrained fluid versus the wetted surface area A_w of the solid refrigerant:

$$D_h = 4\frac{V_r - V_s}{A_w} \tag{17}$$

For spherical particles of an average particle diameter D_p the hydraulic diameter is:

$$D_h = \frac{2}{3}D_p\frac{\alpha}{1-\alpha} \tag{18}$$

Flow across through the regenerator is dictated by some mass flow $\dot{m}$ which is a function of time. This is defined by the superficial fluid velocity, v_r, entering the regenerator with a cross-sectional area, A_r, at the interface. This can also be discussed as a volumetric flux:

$$\dot{m}(t) = \rho_f A_r v_r(t) \tag{19}$$

$$\dot{V}(t) = A_r v_r(t) \tag{20}$$

Due to mass continuity, the pore velocity or peak fluid averaged velocity is determined by the porosity:

$$v_p = \frac{v_r}{\alpha} \tag{21}$$

The steady-state Reynolds number can be defined in two ways, either particle scale or hydraulic scale respectively:

$$Re_p = \frac{\rho_f D_p v_r}{\mu_f} \tag{22}$$

$$Re_h = \frac{\rho_f D_h v_p}{\mu_f} \tag{23}$$

2.2.2. Pressure Drop

The regenerator has been discussed as a thermal resistor but can also act as a hydraulic resistor translating into a pressure drop for a given mass flux across the matrix. This resistance is

characterized by an equivalent friction factor, F, derived from the Darcy expression for losses due to wall effects for packed beds [15]:

$$F = \frac{2D_h}{\rho_f {v_p}^2}\left|\frac{\Delta P}{L}\right| \tag{24}$$

The most commonly used expression for pressure drop across a packed bed is the Ergun relationship [16]:

$$\left|\frac{\Delta P}{L}\right| = 150\frac{(1-\alpha)^2}{\alpha^3}\frac{\mu_f}{{D_p}^2}v_r + 1.75\frac{(1-\alpha)}{\alpha^3}\frac{\mu_f}{D_p}{v_r}^2 \tag{25}$$

This is an empirical relationship that has been proven to be remarkably accurate. The Ergun correlation does, however, tend to under-predict the pressure drop in smaller regenerators due to higher proportional friction affects from the chamber wall and a locally higher porosity value. Under high frequency cyclic flow conditions, inertial effects may be induced. Pumping power can be found from the pressure drop and the volumetric flux:

$$\dot{W}_{pump} = \dot{V}|\Delta P| \tag{26}$$

2.2.3. Heat Transfer Modes

The functional purpose of a passive regenerator relies on the convective heat transfer between the fluid and solid; however, this is not sufficient to describe the thermal behaviour of a passive regenerator. A set of transport processes occur simultaneously on different length scales within the regenerator that must be accounted for:

- Conduction of thermal energy from the surface of the particle to its interior
- Longitudinal thermal conduction within the solid along the regenerator
- Advective thermal transport or enthalpy flux due to fluid flow
- Dispersion in the regenerator which acts to mix the fluid within the matrix
- Viscous dissipation acts a thermal source within the regenerator

The imperfect heat transfer within the regenerator can be partially captured by an effective conductive flux along the regenerator through the fluid and solid as well as a coupled convective flux between the fluid and solid. Expressions for these effects can be found from traditional heat transfer theory. The net conductive heat flux within the fluid or solid is described by Fourier's Law and an effective thermal conductivity, k_{eff}:

$$Q_k = -k_{eff} A \frac{\partial T}{\partial x} \tag{27}$$

The convective heat flux per unit length between the fluid and solid respectively are described by Newton's law of cooling:

$$Q'_{\bar{h}} = \bar{h} A'_w \left(T_f - T_s\right) \tag{28}$$

where $\bar{h}$ is the local average convection coefficient, A'_w is the wetted area per unit length and $\left(T_f - T_s\right)$ is the local temperature difference between the fluid and solid.

2.2.4. Effectiveness

The effectiveness of a passive regenerator is a measure of the temperature variation in the fluid observed at the boundary interfaces. In the case of the perfectly effective regenerator, the fluid temperature leaving the regenerator during a blow period is at equilibrium with the reservoir temperature. This can be considered to be an infinite thermal resistance between the two reservoirs. Conversely, when discussing ineffectiveness, the variation in temperature observed at the interface between the cold and hot blows results in an effective heat leak through the regenerator. Refer back to Figure 1 which depicts variable effectiveness.

2.3. Active Regenerators

Unlike passive regenerators, active regenerators have a work mode induced by the externally applied magnetic field. This forces variations in the enthalpy flux through the

regenerator. Otherwise, the governing equations for transient heat transfer within the regenerator would be the same as those for a passive regenerator. The governing equations for the active magnetic regenerator consider the solid and fluid phases separately. External mechanical components such as fluid pumps, heat exchangers, and the magnetic field generator are required for a functional system but are considered as secondary elements and are discussed in subsequent chapters. The instantaneous energy equations are derived by considering an infinitesimal slice, dx, in the regenerator. This approach relies on the assumption that one spatial dimension parallel to the flow direction dominates and is sufficient to describe the energy interactions within the volume [5]. The boundary fluxes across the control volume are considered and depicted in Figure 6.

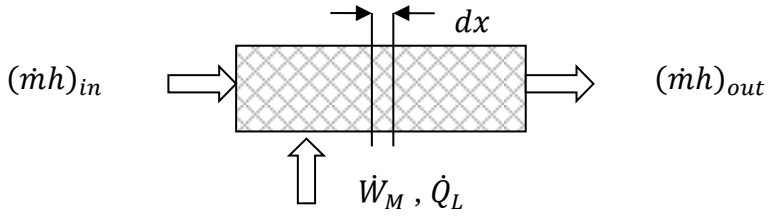

Figure 6: Boundary fluxes considered over the MCM regenerator.

The energy transfers across the boundaries include the fluid enthalpy flux due to mass flow, $\dot{m}h$, the magnetization work rate due to applied magnetic field, $\dot{W}_M$, and a heat leak from the environment, $\dot{Q}_L$. An adiabatic transverse boundary condition is often assumed which eliminates any heat loss to the environment (i.e. $\dot{Q}_L = 0$). Environment losses and other entropy generation mechanisms will be discussed later on.

2.3.1. Heat Transfer Fluid Governing Equations

The HTF is considered as an incompressible simple fluid with viscous losses that are insignificant in the energy balance. The net energy balance expression for the fluid over the entire regenerator volume can be written:

$$\frac{dU_f}{dt} + (\dot{m}h)_{out} - (\dot{m}h)_{in} = -\delta\dot{Q}_{k,f} + \dot{Q}_{\bar{h},f} \tag{29}$$

The terms on the left side of the equality describe the net rate of change of internal energy of the entrained fluid and the enthalpy fluxes across the boundaries. The terms on the right describe the net conductive heat flux through the fluid and the convective heat flux between the solid and fluid. The instantaneous energy expression for the fluid at a given location within the regenerator can be found by converting Equation (29) into specific mass and length quantities over the infinitesimal volume:

$$m_f' \frac{\partial u_f}{\partial t}\partial x + \dot{m}\frac{\partial h_f}{\partial x}\partial x = -\frac{\partial \dot{Q}_{k,f}}{\partial x}\partial x + \dot{Q}'_{\bar{h},f}\partial x \tag{30}$$

The m_f' term can be expressed by the total fluid mass over the regenerator length, L. Equation (30) simplifies to:

$$\frac{m_f}{L}\frac{\partial u_f}{\partial t} + \dot{m}\frac{\partial h_f}{\partial x} = -\frac{\partial \dot{Q}_{k,f}}{\partial x} + \dot{Q}'_{\bar{h},f} \tag{31}$$

Internal energy and enthalpy for a fluid can be related to temperature and pressure using the fundamental relations:

$$du_f = Tds - Pdv \tag{32}$$

$$dh_f = Tds + vdP \tag{33}$$

As previously stated, the fluid is considered incompressible, which implies $dv = 0$. It is also assumed that viscous losses are negligible over the infinitesimal volume which implies $dP \cong 0$. Note that viscous losses associated with pressure drop are a significant factor in machine operation but are neglected in fundamental AMR theory to ascertain the temperatures of each phase. Under these simplified conditions, the internal energy and enthalpy are equivalent to the

entropy change in the fluid. This also allows for a single specific heat capacity function to be used that is only dependent on temperature, $c_f = c_v = c_P$.

$$du_f = dh_f = c_f dT_f \tag{34}$$

Substituting Equation (27), (28) and (34) into equation (31) yields the governing expression for the fluid energy balance:

$$\frac{m_f c_f}{L}\frac{\partial T_f}{\partial t} + \dot{m} c_f \frac{\partial T_f}{\partial x} = \frac{\partial}{\partial x}\left(k_f A_f \frac{\partial T_f}{\partial x}\right) + \bar{h} A'_w \left(T_s - T_f\right) \tag{35}$$

2.3.2. Solid Refrigerant Governing Equations

A net energy balance can be written similarly for the solid MCM refrigerant:

$$\frac{dU_s}{dt} = -\delta \dot{Q}_{k,s} + \dot{Q}_{\bar{h},s} - \dot{W}_M \tag{36}$$

The term on the left side of the equality describe the net rate of change of internal energy of solid. The terms on the right describe the net conductive heat flux through the solid, the net convective heat flux between fluid and solid, and the magnetic work rate. This last term can be written using Equation (1):

$$\delta \dot{W}_M = -BV\frac{dM}{dt} = -BA\partial x \frac{dM}{dt} \tag{37}$$

The instantaneous energy expression for the solid at a given location within the regenerator can be found by introducing (37) into (36) and converting to specific mass and length quantities over the infinitesimal volume:

$$m'_s \frac{\partial u_s}{\partial t}\partial x = -\frac{\partial \dot{Q}_{k,s}}{\partial x}\partial x + \dot{Q}'_{\bar{h},s}\partial x + m'_s B \frac{\partial \overline{m}}{\partial t}\partial x \tag{38}$$

The magnetization term is rewritten as mass magnetization, $\overline{m} = \frac{M}{\rho}$. The m'_s term can be found from the total solid mass divided over the regenerator length, L or by $m'_s = \rho A$. Equation (38) simplifies to:

$$\frac{m_s}{L}\frac{\partial u_s}{\partial t} = -\frac{\partial \dot{Q}_{k,s}}{\partial x} + \dot{Q}'_{\bar{h},s} + \frac{m_s B}{L}\frac{\partial \bar{m}}{\partial t} \tag{39}$$

The specific internal energy term, including the thermal and magnetic constituents, can be written from Equation (11):

$$du = c_B dT + T\left.\frac{\partial \bar{m}}{\partial T}\right|_B dB + B d\bar{m} \tag{40}$$

Combining (40) into (39) yields:

$$\frac{m_s c_B}{L}\frac{\partial T_s}{\partial t} + \frac{m_s T_s}{L}\left.\frac{\partial \bar{m}}{\partial T}\right|_B \frac{\partial B}{\partial t} + \frac{m_s B}{L}\frac{\partial \bar{m}}{\partial t} = -\frac{\partial \dot{Q}_{k,s}}{\partial x} + \dot{Q}'_{\bar{h},s} + \frac{m_s B}{L}\frac{\partial \bar{m}}{\partial t} \tag{41}$$

It can be seen that the magnetic work term appears on both sides of the balance expression leaving only the magnetic entropy response. This can be interpreted as the applied magnetic work being held in the material in the magnetized state and subsequently released in the demagnetized state. The thermal entropy change due to the change in magnetization state is of actual interest for the regenerator balance. Combining the heat transfer equations from (27) and (28) yields the governing expression for the solid energy balance:

$$\frac{m_s c_B}{L}\frac{\partial T_s}{\partial t} + \frac{m_s T_s}{L}\left.\frac{\partial \bar{m}}{\partial T}\right|_B \frac{\partial B}{\partial t} = \frac{\partial}{\partial x}\left(k_s A_s \frac{\partial T_s}{\partial x}\right) + \bar{h} A'_w \left(T_f - T_s\right) \tag{42}$$

2.4. The Idealized Cycle

This idealized AMR cycle implies perfectly effective regeneration as well as a sufficiently large convection coefficient such that the solid and fluid phases are constantly at equivalent temperatures, $T_s \cong T_f = T(x,t)$ therefore only a single temperature variable is required to describe the fluid and solid. Under this assumption, equations (35) and (42) can be combined into a single partial differential equation:

$$\frac{\left(m_s c_B + m_f c_f\right)}{L}\frac{\partial T}{\partial t} = -\dot{m} c_f \frac{\partial T}{\partial x} - \frac{m_s T}{L}\left.\frac{\partial \bar{m}}{\partial T}\right|_B \frac{\partial B}{\partial t} + \frac{\partial}{\partial x}\left(k_{eff} A \frac{\partial T}{\partial x}\right) \tag{43}$$

The thermal conductivities of the fluid and solid are replaced by a single effective value, k_{eff}, which is the addition of the static conductivity of the regenerator bed and a convective component within the regenerator [17] [18].

2.4.1. Temperature Profile

A further idealization is to assume the axial conduction term is small relative to the others as it is second order in temperature while the others are first order. Conductive losses can be incorporated later in the overall energy balance. The approach proposed by Rowe [5] suggests to normalize the expression by the refrigerant thermal mass and non-dimensionalize both the time coordinate by the blow period, $t = \tau_B \hat{t}$, and the spatial coordinate by the length, $x = L\hat{x}$. Neglecting the thermal conductivity and normalizing (43) yields:

$$0 = \left(1 + \frac{m_f c_f}{m_s c_B}\right)\frac{1}{\tau_B L}\frac{\partial T}{\partial \hat{t}} + \frac{\dot{m} c_f}{m_s c_B L}\frac{\partial T}{\partial \hat{x}} + \frac{T}{c_B \tau_B L}\frac{\partial \bar{m}}{\partial T}\bigg|_B \frac{\partial B}{\partial \hat{t}} \tag{44}$$

$$0 = \left(1 + \frac{m_f c_f}{m_s c_B}\right)\frac{\partial T}{\partial \hat{t}} + \frac{\dot{m} c_f \tau_B}{m_s c_B}\frac{\partial T}{\partial \hat{x}} + \frac{T}{c_B}\frac{\partial \bar{m}}{\partial T}\bigg|_B \frac{\partial B}{\partial \hat{t}} \tag{45}$$

A thermal mass ratio, R, and thermal utilization, Φ, are introduced in Equations (46) and (47) below. Equation (14) defining adiabatic temperature change is rewritten using mass magnetization, $\bar{m}$, in (48).

$$R \equiv 1 + \frac{m_f c_f}{m_s c_B} \tag{46}$$

$$\Phi \equiv \frac{\dot{m} c_f \tau_b}{m_s c_B} = \frac{m_d c_f}{m_s c_B} \tag{47}$$

$$dT_{ad} = -\frac{T}{c_B}\frac{\partial \bar{m}}{\partial T}\bigg|_B dB \tag{48}$$

Introducing these relationships and neglecting conductive losses, Equation (45) can be consolidated to a simplified differential equation for temperature profile within the regenerator:

$$0 = \frac{\partial T}{\partial \hat{t}} + \frac{\Phi}{R}\frac{\partial T}{\partial \hat{x}} - \frac{1}{R}\frac{\partial T_{ad}}{\partial \hat{t}} \tag{49}$$

2.4.2. Analytic Energy Balance

The idealized cycle energy balance is derived from a control volume analysis around the active regenerator under cyclic steady-state heat pumping conditions. Recalling Figure 2, the four state points of the AMR cycle are depicted. At cyclic steady-state operation, it is assumed that the average temperatures at the regenerator ends (T_{a0} and T_{a1}) are enough to define the state point a in the AMR cycle. Figure 7 portrays the instantaneous temperature distribution and energy flow through the regenerator at the start of the cold blow.

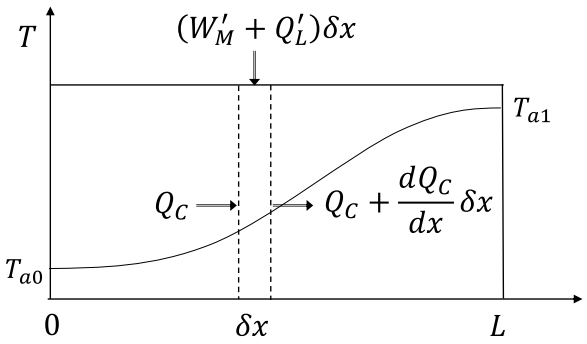

Figure 7: Representation of the energy balance over an infinitesimal volume of the regenerator.

Examining the net effects per unit length over an infinitesimal volume of the regenerator gives:

$$W'_M + Q'_L = \frac{dQ_C}{dx} \tag{50}$$

Simplified analytical expressions for work and cooling have been developed from Equation (50) that further reduces the complexity of the governing Equation (43) for the case of ideal magnetocaloric effect as a function of temperature [18] [19]. A constant specific heat capacity value is assumed for the solid (i.e. $c_s = c_B = \text{constant}$). The analytic expression for local regenerator cooling power is given by the boundary temperatures at the start of the hot blow, T_{a0} and T_{a1},

$$\dot{Q}_C = \frac{m_s c_s}{\tau_c}\frac{\Phi}{R}\left(\frac{\Delta T_{ad}}{T}\right)T_{a0}\left[1 - \frac{p}{\sin(p)}\left(\frac{\Phi}{\kappa R}\frac{\Delta T_{ad}}{T}\right)^{-1}\left(\frac{T_{a1}}{T_{a0}} - \cos(p)\right)\right] \quad (51)$$

and the local magnetic work rate per unit length is found by,

$$\dot{W}'_M = \frac{m_s c_s}{L\tau_c}\left(\frac{\Delta T_{ad}}{T}\right)\left[\frac{R-1}{R}\left(\frac{\Delta T_{ad}}{T}\right)\int_0^1 T d\hat{x} + \frac{\Phi}{R}(T_{a1} - T_{a0})\right] \quad (52)$$

and the transverse heat leaks to the regenerator are modelled by,

$$\dot{Q}'_L = \frac{\sigma}{L}(T - T_\infty) \quad (53)$$

where σ is the effective conductance loss coefficient. The non-dimensional internal thermal conductance is defined as,

$$\kappa \equiv \frac{\tau_B}{m_s c_s}\frac{k_{eff} A_r}{L} \quad (54)$$

And the p term is defined as,

$$p \equiv \left(\frac{\Delta T_{ad}}{T}\right)\left(\frac{1}{\kappa}\frac{R-1}{R}\right)^{1/2} \quad (55)$$

Note that the expressions for magnetic and cooling power are functions of the adiabatic temperature gradient, $\frac{\Delta T_{ad}}{T}$. With single MCMs, this parameter varies within the regenerator both spatial and temporally. It interesting to note that all the other terms in the expressions are either measurable or define characteristics of the cycle.

2.4.2.1. Adiabatic Temperature Gradient

If the adiabatic temperature change of a MCM is plotted over a range of initial temperature conditions, the magnetocaloric effect (MCE) curve for the given material as a function of field strength is found. As an example, the MCE curve for gadolinium at different field strengths is presented in Figure 8.

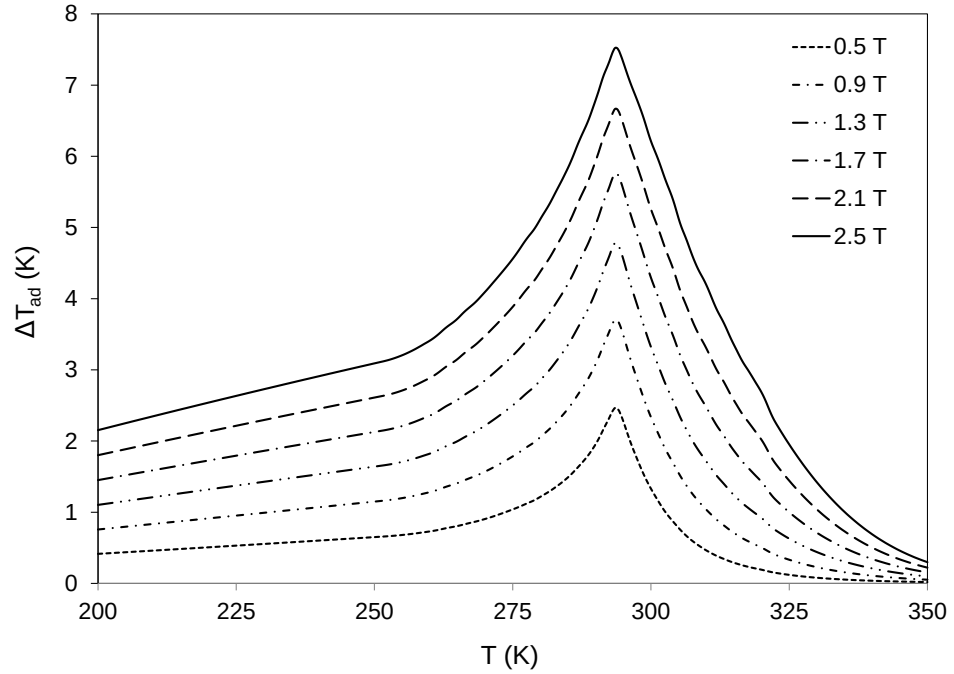

Figure 8: The MCE curve for gadolinium at different magnetic field strengths.

It is valuable to understand how this measurable data for a refrigerant corresponds to the change in temperature of the heat transfer fluid and the subsequent enthalpy flow through the regenerator. The temperature variation of the cold reservoir due to the enthalpy flow from the active regenerator, ΔT_C, can be deduced from a simple entropy balance on the HTF. The net entropy flow of the HTF to the cold reservoir can be written as:

$$\dot{S}_C = \frac{\dot{Q}_C}{T_C} = \frac{m_d c_f}{\tau_c} \frac{\Delta T_C}{T_C} \tag{56}$$

Providing the convective heat transfer and thermal mass of the regenerator are significantly large, then the temperature change of the fluid can be assumed equal to that of the MCE,

$$\Delta T = \Delta T_{ad}(T) \tag{57}$$

Again, regarding the ideal case, the entropy flows in and out of the regenerator at the cold and hot reservoirs respectively are equal using Equation (57),

$$\dot{S}_C = \dot{S}_H \tag{58}$$

$$\frac{\Delta T_C}{T_C} = \frac{\Delta T_H}{T_H} \tag{59}$$

$$\left.\frac{\Delta T_{ad}(T_H)}{T_H}\right|_{MCE} = \left.\frac{\Delta T_{ad}(T_C)}{T_C}\right|_{MCE} \tag{60}$$

This result suggests that for an ideal AMR, $\frac{\Delta T_{ad}}{T}$ should be constant. In the real case, the MCE varies with temperature thereby these values will not be equivalent depending on the operating location on the MCE curve. During operation, the AMR exists at different temperatures both spatially within the matrix and temporally throughout a cycle meaning the gradient is also varied at any location or instant.

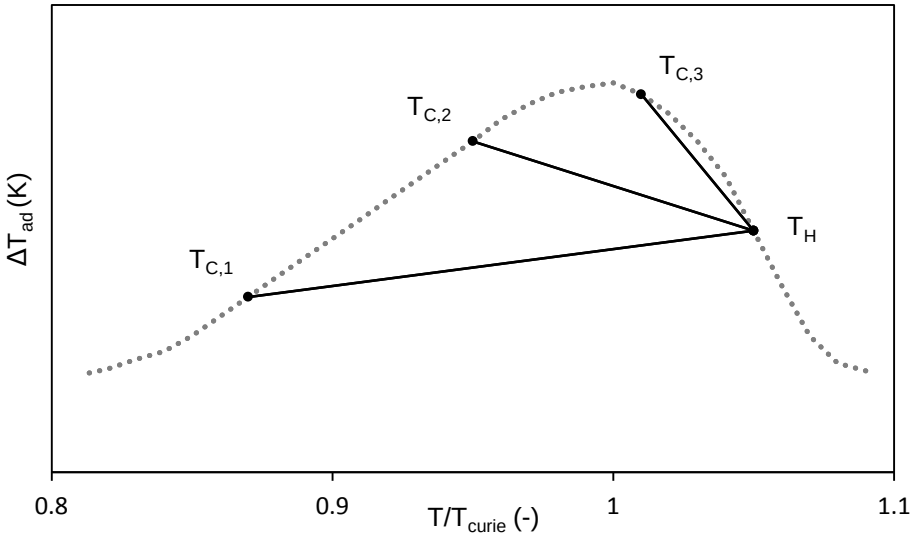

Figure 9: Adiabatic temperature gradient representation shown on a genetic MCE curve.

Figure 9 is a representative image of an MCE curve with the reference temperature of the adiabatic temperature change normalized by the Curie temperature so that it can be interpreted generically for any MCM. Three different cold zone temperatures are shown relative to one hot zone temperature. In practice, the reservoir temperatures are often the only measurements available. The slope of the connecting lines can be interpreted as an *effective gradient* for a given

set of operating conditions, T_C and T_H, wherein using the ideal assumption, the line would obey equation (60). Figure 9 is intended to illustrate that the adiabatic temperature gradient is not constant as equation (60) indicates. It can be inferred that some minimum entropy flux condition would exist within the process. This minimum may act as a limiting factor for overall entropy flow.

2.4.2.1. Thermal Mass Ratio (R)

The thermal mass ratio as defined by equation (46) compares the thermal mass of the fluid volume entrained in the pores of the regenerator to that of the solid refrigerant volume. This value is dependent on regenerator morphology and the thermal properties of both the solid and fluid. When $R > 1$, the entrained fluid acts as a parasitic load on the system in effect, reducing the useful temperature change generated by the magnetic field. To give an example, $R \approx 2$ for a regenerator comprised of ~300 μm gadolinium spheres with a porosity of ~0.35 where water is the HTF. When $R \cong 1$, which can be achieved with low thermal mass gases or high specific heat solids, the temperature distribution within the regenerator is well approximated as a linear [19]. In this case, with ideal MCE scaling and $p = 0$ Equations (51) can be further simplified to:

$$\dot{Q}_C = \frac{m_s c_s}{\tau_c} \Phi \left(\frac{\Delta T_{ad}}{T} \right) T_C \left[1 - \left(\frac{\Phi}{2} + \left(\frac{\Phi}{\kappa} \frac{\Delta T_{ad}}{T} \right)^{-1} \right) \left(\frac{T_H}{T_C} - 1 \right) \right] \tag{61}$$

2.5. Summary

This chapter presents the state equations for a magnetic solid and discusses the MCE, heat capacity and temperature response due to applied magnetic field. The thermo-hydraulic behaviour of passive regenerators is outlined. Next, two-phase energy equations are derived that describe the instantaneous energy state of the solid and fluid at a given location within an active regenerator. Simplifications are assumed to reduce the complexity of this approach to capture

bulk energy transport effects over a full AMR cycle. Analytic expression for cooling power and magnetic work are presented. The effective adiabatic temperature gradient is defined and explained. These analytic expressions allow operational performance to be modeled quickly as they are computationally basic. Providing the accuracy is reasonable, these expressions are ideal for a thorough examination of the parameter space when conducting device design.

Chapter 3: Design Principles and Performance Metrics

The previous chapter presents fundamental theory that describes the physical behaviour of active magnetic regenerators as well as the energy transport expressions for the AMR cycle. Simplified analytical expressions are presented for the cycle-averaged cooling power and magnetic work. With the necessary theory identified, a strategy for employing this theory in the design process of a real machine is now desired. This chapter proposes a framework for approaching device design that incorporates the analytic expressions. The higher level expressions (i.e. the transient equations for the fluid and solid phases) could also be used, however; they would be more computationally intensive. The framework focuses on the dominant attributes and principles associated with implementing the AMR cycle in a real device. Each design factor will be discussed independently; however, no single factor is entirely independent from the others. Metrics for gauging the functional performance of a device are also presented.

3.1. The Real Machine

A physical refrigerator system consists of more than an active magnetic regenerator. In a macroscopic sense, the AMR refrigerator can be approached like a classic simple refrigerator. A schematic representation of the refrigerator is shown in Figure 10(a) where the refrigeration core is the AMR, fluid displacer and magnet system. A simplified representation of the refrigerator core is shown in Figure 10(b).

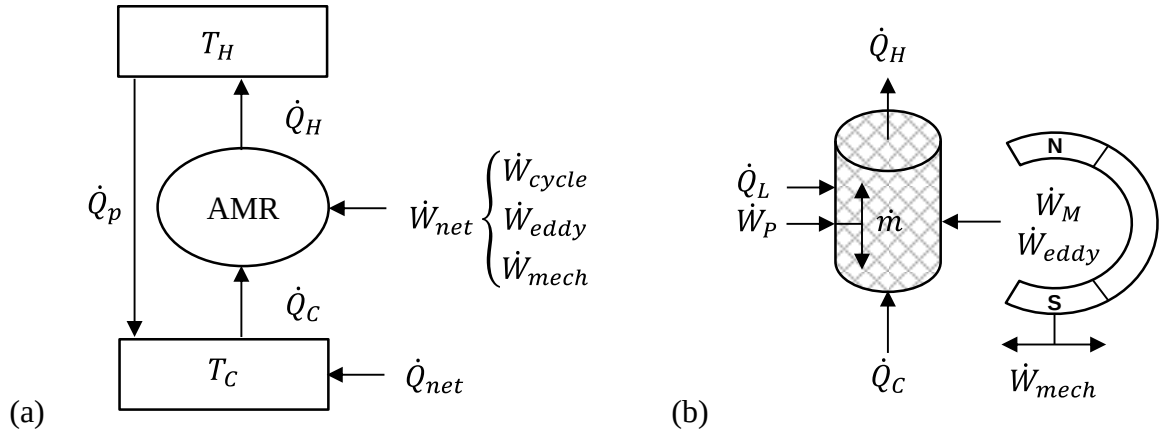

Figure 10: (a) Environmental scale representation of an AMR refrigerator. (b) Simplified machine scale representation of an AMR refrigerator.

Work input drives heat from a cold zone to a heat rejection reservoir with various loss mechanisms that increase net input work and a decrease net cooling power. The applied or net cooling power of the machine is found using measured experimental data while parasitic environmental losses can be estimated through modeling or experimentation. The heat rejection temperature and cold zone temperature are also measurable quantities.

3.1.1. Cooling Power

The cooling power of the AMR cycle, $\dot{Q}_C$, describes the time-averaged enthalpy moved across the matrix by the HTF from the cold zone. The thermal leak to the regenerator, $\dot{Q}_L$, is present in the analytic energy balance of equation (50) and reduces the cooling potential of the regenerator, $\dot{Q}_C$, which is described by equation (51). This internal leak to the regenerator is due to imperfect isolation from the surroundings as well as the eddy current thermal dissipation within the solid. At the machine scale, the total net cooling, $\dot{Q}_{net}$, is the potential cycle cooling power, $\dot{Q}_C$, less the environmental heat leak, $\dot{Q}_p$, on the cold zone:

$$\dot{Q}_{net} = \dot{Q}_C - \dot{Q}_p \tag{62}$$

In the case of no applied heat load ($\dot{Q}_{net} = 0$) and perfect thermal isolation of the regenerator ($\dot{Q}_L = 0$), the device will still have to pump some environmental heat load to achieve a temperature span. The refrigerator will reach cyclic steady-state operating conditions when the total thermal load is balanced by the cooling of the AMR. At these conditions, the maximum temperature span is observed. Note that fluid volume between the cold-side regenerator interface and the heat exchanger where the thermal load is absorbed from can have a negative impact on the temperature span. This is particularly so if the fluid volume is stagnant during flow oscillation and does not arrive at the heat exchanger.

3.1.2. Work Modes

The input power required to drive the thermodynamic cycle, $\dot{W}_{cycle}$, is the sum of two constituents:

$$\dot{W}_{cycle} = \dot{W}_M + \dot{W}_P \tag{63}$$

The magnetic work rate term, $\dot{W}_M$, describes the power associated with magnetizing the refrigerant and is found from (52) for an ideal MCM with no hysteresis. The reversible work rate can be reduced due to demagnetization fields which impact the expected variation in magnetization. The pumping term, $\dot{W}_P$, describes the power needed to displace the HTF across the regenerator matrix which is dictated by the pressure drop and is found from equation (26). In a real machine, hydraulic losses external to the regenerator do exist; however, the regenerator tends to dominate this effect. The Ergun relationship of Equation (25) is sufficient to describe pressure drop through a matrix but as previously stated, tends to under predict experimental measurements.

The total net input work rate, $\dot{W}_{net}$, includes the cycle work rate plus the device scale losses:

$$\dot{W}_{net} = \dot{W}_{cycle} + \dot{W}_{eddy} + \dot{W}_{mech} \quad (64)$$

Mechanical input, $\dot{W}_{mech}$, describes the power required to move the magnet or regenerator with respect to the other along with any friction and inertial forces. Eddy currents, which are stray electrical currents induced in conductive material by changes in the magnetic flux may also be present. Eddy currents generate forces that oppose the changing magnetic field resulting in an additional power dissipation mode, $\dot{W}_{eddy}$.

3.2. Performance Metrics

To evaluate the performance of an AMR system, one must clearly specify what is being measured. This section discusses how performance of a magnetic refrigerator is assessed from the modes of work and heat transfer as well as the operational temperatures. A variety of performance metrics are defined depending on where the system boundary is placed and what crosses the boundary.

3.2.1. First Law Metric: COP

The coefficient of performance (COP) is a standard metric used in the refrigeration community. COP is a first law efficiency rating. It is a meaningful rating within the vapour-compression industry because it is defined under standardized conditions. For example, measurements of cooling power are conducted at specified evaporator and condenser temperatures. COP has limited value when used to describe AMR performance when no definition of standardized testing exists. Based upon the previous discussion of the various power requirements and the total thermal load on the AMRs, a number of different COP definitions are possible [20].

$$COP_{device} = \frac{\dot{Q}_{net}}{\dot{W}_{net}} \quad (65)$$

$$COP_{config} = \frac{\dot{Q}_{net}}{\dot{W}_{cycle}} \tag{66}$$

$$COP_{cycle} = \frac{\dot{Q}_C}{\dot{W}_{cycle}} \tag{67}$$

The overall performance of an AMR machine is represented by COP_{device}; this metric could vary dramatically between devices using the same field and refrigerant. COP_{config} can be considered the performance of a particular AMR device configuration. An example of where this might be useful is the comparison of two devices operating with the same amount of refrigerant at the same operating conditions, but one is rotary while the other is reciprocating. COP_{cycle} focuses on the regenerator only and disregards the fact that heat being pumped to the hot reservoir may not be useful cooling. This last metric is useful in that it allows direct comparisons between the effects of MCM type, matrix geometry, and multi-material layering. One could also use this metric to meaningfully compare the regenerator performance in different devices. A regenerator design that gives a large value for COP_{cycle} might be used in any number of other devices with different geometries. One can then focus on identifying the best device design somewhat decoupled from the regenerator.

3.2.2. Second Law Metrics: Exergy and FOM

While COP can be an adequate way to compare similar AMR refrigerators operating under like operating conditions, it does not capture performance for all the services desired. A first law-type rating like COP does not account for the temperature span between the cold zone and heat rejection reservoir which is highly relevant for a refrigerator. For instance, a high cooling power can be achieved with no temperature span. This would result in a high COP but most refrigeration applications require some temperature span. Often for AMR results, cooling power and temperature span follow a nearly linear inverse relationship (i.e. high span equates to

low cooling power and vice versa). Equivalent to the Carnot minimum work requirement of a heat pump or the reversible work rate, the useful cooling power can be described by its exergetic equivalent:

$$\dot{W}_{rev} = \dot{E}x_Q = \dot{Q}\left(\frac{T_H}{T_C} - 1\right) \tag{68}$$

The exergetic cooling power, $\dot{E}x_Q$, describes both the amount of heat pumped and the temperature span generated. $\dot{E}x_Q = 0$ if either $\dot{Q} = 0$ or $T_C = T_H$. This expression can indicate a balance point between cooling power and temperature span.

A figure of merit (FOM) can be defined that compares the ideal power requirement to the actual power input; entropy generation due to mechanical and physical losses dictate this metric:

$$FOM = \frac{\dot{E}x_Q}{\dot{W}} = COP\left(\frac{T_H}{T_C} - 1\right) \tag{69}$$

FOM is a second law type efficiency and is a more encompassing metric that COP. Various definitions of FOM can be found based on a specific COP definition. If the device level definition is considered, the net cooling power is of interest and the work rate can be discussed in terms of the reversible and irreversible inputs:

$$FOM_{device} = \frac{\dot{E}x_{Q_{net}}}{\dot{W}_{net}} = \frac{\dot{E}x_{Q_{net}}}{\dot{W}_{rev} + \dot{W}_{irr}} \tag{70}$$

$$\dot{W}_{irr} = \dot{W}_P + \dot{W}_{mech} + \dot{W}_{eddy} \tag{71}$$

The irreversible work rate, $\dot{W}_{irr}$, is the sum of the pumping power, $\dot{W}_P$, due to viscous dissipation, the mechanical power, $\dot{W}_{mech}$, due to friction and the eddy current power, $\dot{W}_{eddy}$, due to eddy current dissipation. Based on the definition of exergetic cooling potential, FOM_{device} can be rewritten as:

$$FOM_{device} = \left(1 + \frac{\dot{W}_{irr}}{\dot{E}x_Q}\right)^{-1} \tag{72}$$

3.2.3. Cost Metric: Specific Cooling

Cooling power can be increased by either using more refrigerant or higher magnetic field strengths; however, by increasing these, there is almost always an in increase in cost. In fact, these two elements tend to dominate the capital cost of a device. COP and FOM present the thermodynamic efficiency of a device. It is also advantageous to compare the relative cooling of different systems by the amount of refrigerant used and the high field strength. The *specific exergetic cooling power*, $\bar{\mu}$, is suggested by Rowe [9] and is defined here as:

$$\bar{\mu} \equiv \frac{\dot{E}x_Q}{\bar{B}_h V_s} \tag{73}$$

$\bar{B}_h$ is the mean high magnetic flux density and V_s is the total volume of refrigerant. Note that FOM can also be converted into a specific form in the same manner.

3.3. The Design Framework

The device design framework presented here follows a synthesis method or bottom-up design approach that can be visualized in Figure 11. Identifying the intended application and scale of implementation is critical to the design process. The final services to be delivered by the refrigerator are the net cooling power of the device, $\dot{Q}_{net}$, and the temperature span between reservoirs, T_H and T_C. Once these factors have been identified, many design variables will become inapplicable and the scope of the design space will be reduced. Simply providing these services is only a portion of the final design. Delivering the services effectively with high performance is also desired.

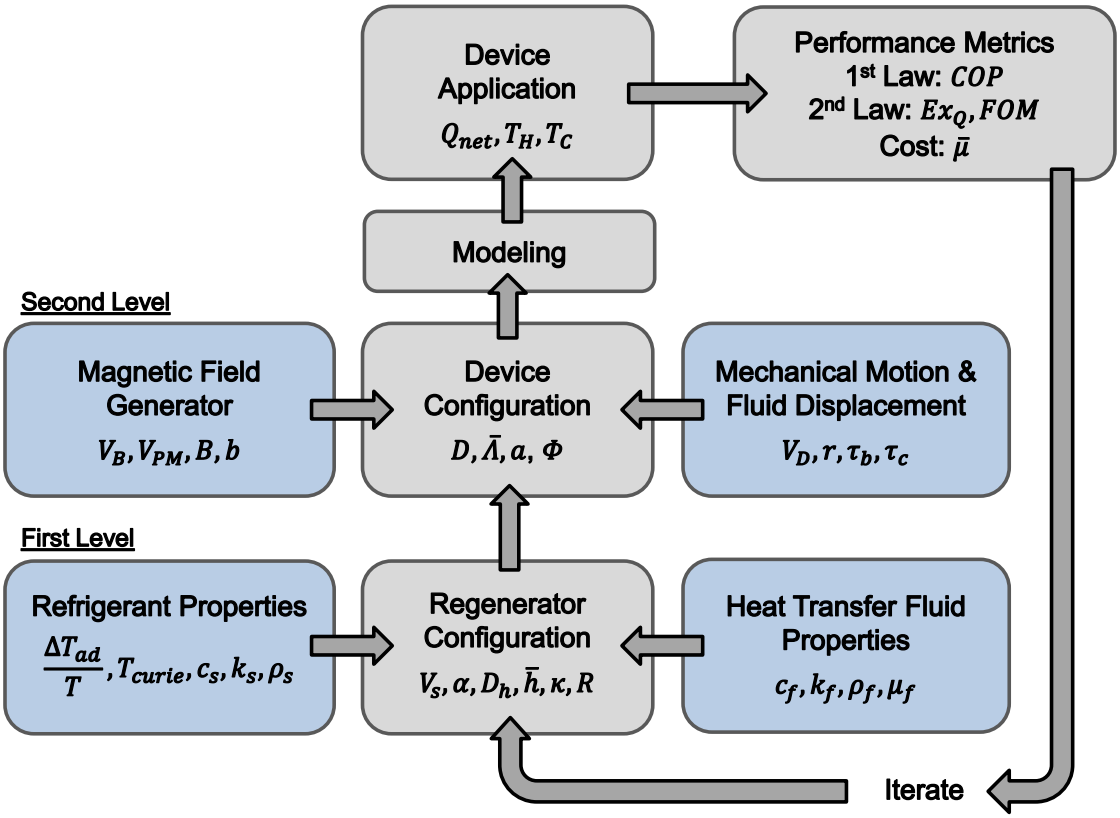

Figure 11: Design framework for magnetic refrigerator development shown as an iterative process.

The methodology for approaching device design using the framework described in Figure 11 suggests that firstly, the intended device application requirements and an acceptable threshold of performance must be specified. Now design decisions can be made regarding the first level elements. These are the primary constituents of the AMR regenerator namely the refrigerant and heat transfer fluid. These are combined into active regenerators in some specific morphology or configuration. With the core of the AMR defined, specifically the active regenerator, selections regarding the machine elements can be made. The second level elements namely the magnetic field generator and the system mechanisms that define motion type and fluid displacement are combined with the active regenerator into some device configuration. The operation of a device based on all these parameter choices then must be modeled and compared to the initial desired

application. Numerous numerical methods exist to estimate the operational behaviour of the AMR cycle [2]. Models that exist vary in complexity depending on which governing equations are used and what level of detail is included in terms of physical effects other that the magnetocaloric response of the solid and the heat transport of the fluid. The analytic expressions from Chapter 2 can also be applied at this stage. If the application is met, the performance of the design is evaluated using the appropriate metrics and, if need be, the process is reiterated to reach the specified performance requirements.

3.4. First Level Design Factors

The first level of design focuses on the elemental constituents of the active regenerator and the AMR cycle. The two thermodynamic substances involved in the process, the solid refrigerant and heat transfer fluid, interact within the regenerator geometry. This section describes the practical features of the solid and fluid constituents and the available regenerator geometries.

3.4.1. Refrigerant Characteristics

The choices pertaining to the refrigerant are the most critical for defining the cooling potential of an active regenerator. AMR refrigerants are solid materials with intrinsic physical properties including density, heat capacity and thermal conductivity. Available refrigerants are broadly classified as either first-order or second-order materials referencing the nature of their magnetic phase transition. The physical properties of these groups are significantly different meaning the operational behaviour of the refrigerants will also differ greatly. Refrigerant parameters strongly influence the heat transfer between the fluid and solid and dictate the effective conductivity and convection coefficient. They also affect the heat loss due to axial conduction through the regenerator.

Some MCMs can be alloyed and by adjusting the relative composition of the constituents, magnetocaloric properties such as the Curie temperature can be tunable. The magnetic entropy response of the MCM which is described by the adiabatic temperature change and MCE curve is also of interest in this case. An example of a tunable material's MCE is presented in Figure 12.

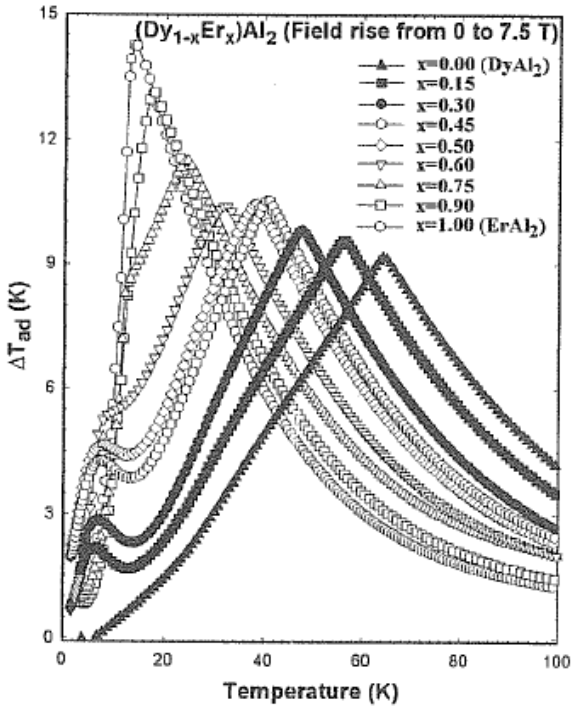

Figure 12: An example of MCE curves for a tuneable material $(Dy_{1-x}Er_x)Al_2$ [21].

3.4.1.1. Layering

Another significant consideration when selecting the refrigerant composition of the regenerator is the option of a layered structure. Layered regenerators consist of more than one refrigerant arranged as sections of the whole. The benefit of this approach is that the cooling potential can be broadened over a larger operating range by arranging a set of MCE curves adjacent to each other [22]. The knowledge regarding layered active regenerators is minimal but growing. There is consequently no prescribed method of constructing these structures. This is an

area of AMR research that is currently receiving a great deal of attention; however, for the purpose of this investigation, layered structures will not be considered.

3.4.1.2. Operating Near the Curie Temperature

The peak magnetic entropy response is observed near the Curie temperature more noticeably in the case of second order materials. When designating materials for an intended operational range of temperatures, it is important that the Curie temperature exists within this range. When the average temperature of the regenerator layer is normalized by the Curie temperature, a non-dimensional temperature is defined:

$$\hat{T} = \frac{T_H + T_C}{2T_{curie}} \tag{74}$$

Experimental evidence suggests that the highest performance is seen in the region of $\hat{T} \cong 1$ meaning the Curie temperature exists half way between the hot-side and cold-side interface temperatures [20].

3.4.2. Heat Transfer Fluid Properties

The cooling potential of an active regenerator cannot be realized without the HTF to move heat outside of the active regenerator. The important physical properties of the HTF include density, viscosity, heat capacity and thermal conductivity. These parameters strongly influence the heat transfer between the fluid and solid and dictate the effective conductivity and convection coefficient. The density and viscosity of the fluid also affect the pressure drop through the matrix. Some commonly used HTFs are presented in Table 1 at specific state points that are possible usage conditions.

Table 1: Properties of some common HTFs are common states of usage.

Parameter	**Helium** (300K, 12atm.)	**Carbon Dioxide** (300K, 12atm.)	**Water** (300K, 4atm.)	**Ethanol** (300K, 4atm.)
Density (kg m^{-3})	2	23	997	785
Specific Heat Capacity (kJ kg^{-1} K^{-1})	5.19	0.94	4.18	2.56
Thermal Conductivity (mJ m^{-1} s^{-1} K^{-1})	157	17	610	165
Viscosity (μPa s)	20	15	854	1050
Thermal Diffusivity (μm^2 s^{-1})	1555	80	15	8
Prandtl Number (-)	0.66	0.82	5.8	16.5

3.4.3. Regenerator Morphology

The choices for regenerator morphology are limited by the manufacturing capabilities associated with the selected refrigerant. As previously listed, passive regenerators have been constructed from crushed irregular particles, spherical particles, parallel platelets, stacked wire mesh, stacked parallel tubes as well as channelled microstructures; however only the first three options are currently applicable to active regenerators due to the current limits of manufacturing; particularly, first-order materials are often brittle and difficult to shape into consistent robust geometries. Porosity and wetted surface area, which is described by the hydraulic diameter, are the parameters of importance to regenerator design. The pressure drop is also determined by these factors which correspond directly to the associated pumping power and the limits on displaced fluid volume and cycle frequency.

Table 2: Features of regenerator structures common to AMRs.

Parameter	**Irr. Particles**	**Spheres**	**Platelets**
Effective Average Diameter (μm)	400 – 800	200 – 600	n/a
Platelet Thickness (μm)	n/a	n/a	450 – 750
Fluid Gap Thickness (μm)	n/a	n/a	250 – 750
Porosity (-)	0.45 – 0.65	0.35 – 0.55	0.25 – 0.65
Hydraulic Diameter (μm)	250 – 1000	100 – 500	250 – 750

It is interesting to note that for platelets to achieve a similar hydraulic diameter to 300 μm spheres, the plate thickness would have to be 100 μm and the gap thickness 50 μm which is very difficult to achieve in manufacturing [23].

3.5. Second Level Design Factors

The second level of AMR machine design focuses on the machine specific elements to drive the AMR cycle. The most influential of these is the magnetic field generator which induces the state change of the refrigerant. This is comparable to the compressor in vapour-compression systems. Other machine elements must be considered. Some type of relative mechanical motion is required to cycle the regenerator between high and low field conditions. Some method of driving the HTF across the regenerator is also required. These elements combined with the regenerator yield some device configuration. A rubric for classifying device configuration is discussed below.

3.5.1. Magnetic Field Generation

While superconducting magnets are an option for cryogenic applications, or industrial scale situations where high cooling powers are required, they are impractical for common scales such as near-room-temperature refrigeration. Superconducting systems are fairly similar in design and usually vary by bore size and maximum possible field strength. There is also an added work consideration with maintaining a superconducting system. For the purposes of this discussion, rating permanent magnet designs for near-room-temperature systems will be addressed solely.

A measure of magnet utilization would be beneficial to quantify the implementation effectiveness of different magnet designs. A magnet utility metric, $\bar{\Lambda}$, is defined here as a means to compare how well different magnetic field generators are implemented in the AMR cycle.

$$\bar{\Lambda} \equiv \frac{V_B(\bar{B}_h - \bar{B}_l)}{V_{PM}} \tag{75}$$

V_{PM} and V_B are the total volumes of the permanent magnet material used in the field generator and the volume of the field region respectively. $\bar{B}_h$ and $\bar{B}_l$ represent the mean high and low magnetic flux densities during the hot and cold fluid blow portion respectively of the cycle and are calculated by:

$$\bar{B}_h = \frac{1}{\tau_{b,H}} \int_0^{\tau_{b,H}} B(t)dt \qquad \bar{B}_l = \frac{1}{\tau_{b,C}} \int_0^{\tau_{b,C}} B(t)dt \tag{76}$$

where τ_b is the blow period. Recall that this period is a fraction of the cycle period, τ_c, which is less than or equal to half ($\tau_b \leq 0.5\tau_c$)To maximize the magnetic utility metric, some primary design objectives can be stated:

- Minimize the volume of permanent magnet material
- Maximize the high field region volume and subsequently, the volume of MCM
- Maximize the high field intensity
- Minimize the low field intensity preferable to an effective value of zero
- Utilize the magnetic material at all times
- Minimize the stray field leakages to the surroundings (This can be accomplished by using flux guiding soft magnetic material [24])

3.5.2. Fluid Displacement Mechanism

The HTF must be displaced cyclically in proper phase with the magnetic cycle to transfer heat to and from the regenerator while maintaining high regenerative effectiveness (i.e. a stable temperature differential). The hot blow occurs when the refrigerant is magnetized to expel heat to the heat rejection reservoir. The cold blow occurs when the refrigerant is demagnetized to absorb heat from the cold zone.

The HTF must always oscillate through the regenerator; however outside the regenerator, the HTF can be displaced through the external flow circuit in either a continuous or modulating fashion. These definitions are linked to the available fluid displacement mechanisms: uni-directional pumps or alternating piston-cylinder-type displacers respectively. In either of these cases, the flow can be controlled and directed by valves (e.g. solenoid, rotary or check). In fact, hybrid systems can be constructed using valves. For the purposes of the classification, continuous flow indicates a uni-directional pump with valve control and modulating flow indicates an alternating displacer. If modulating systems employ valve control or if the fluid oscillations are decoupled from the magnetic cycle, these will be discussed as hybrid flow systems. There are associated advantages and disadvantages to continuous and modulating flow methods. These are compared in Table 3 below.

Table 3: Comparison of benefits of modulating versus continuous flow system.

	Advantages	Disadvantages
Continuous	• Controllable flow waveform • Fluid dwell period achievable during change in magnetic states	• Valves and dynamic sealing is required • Pressure spikes and pumping losses are more prevalent
Modulating	• Simple mechanical implementation • All static sealing is achievable	• Stagnant volumes reduce cooling • Heat exchange effectiveness is reduced • Restricted to regenerator pairs

3.5.3. Mechanical Motion Type

To move the active regenerator between two magnetic states, some relative motion between the regenerator and field generator must occur. The mechanical motion of AMR refrigerators are divided into reciprocating and rotary categories. There are advantages and disadvantages to each arrangement. These are compared in Table 4 below.

Table 4: Comparison of benefits of reciprocating versus rotary mechanical motion.

	Advantages	Disadvantages
Reciprocating	• Controllable magnetic waveform • Dwell period achievable in high and low field states	• Limited to low machine frequency • Often requires mechanism to convert a rotary actuator to linear motion
Rotary	• High machine frequency achievable • Continuous cooling achievable	• Dynamic fluid sealing often required

3.5.4. Device Configuration

The relative configuration and motion type of the regenerator and the magnetic field generator is of interest. These components typically dominate the cost of machine construction. Identical magnet styles can be employed in different configurations; therefore, magnet style cannot be a defining feature exclusively. The configuration will also affect the operating space and the potential performance of the device. In most cases, it is most desirable to maximize the usage of the high field region such that the highest cooling potential can be achieve from the magnet. For these reasons, it is advantageous to use a rubric for classifying these different device configurations. Rowe [9] suggests such a designation number:

$$\mathrm{D} \equiv \frac{r}{bd} \tag{77}$$

where b is number of high field regions used in the system, r is the number of discrete regenerators, and d is the number of regenerators filling a single high field region. In practise, due to unavoidable air gaps, housing thickness etc., d will never be an integer value; however, for the purposes of this classification method, the nearest integer value will be taken. In the majority of cases, d is equal to 1. Exemplary schematic representations of configurations D1 to D4 are shown in Figure 13.

Note that a device with a specific D values need not be like the examples shown here. In terms of the design framework, to achieve high cooling powers, increasing the number of regenerators may be the preferred choice over increasing the mass of the regenerator. Using larger regenerators typically requires using larger magnets which most often increases cost and has an impact on pressure drops which decreases efficiency.

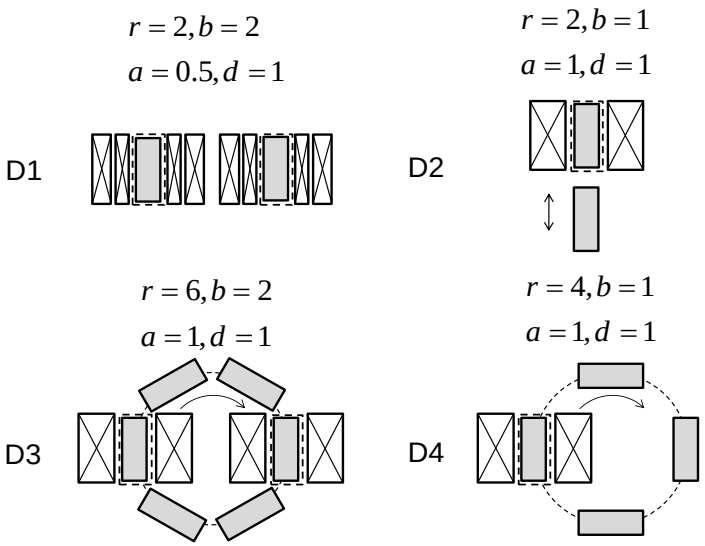

Figure 13: Exemplary representations of device configurations D1-D4 [9].

An additional descriptor is required, a, which is the magnet capacity factor. When examining a single high field region, consider the number of regenerators served by that given field region, r_B. The capacity factor is the ratio of the number of regenerators served per field region to the total number of regenerators in the system.

$$a \equiv \frac{r_B}{r} \tag{78}$$

3.5.4.1. Cycle Frequency

If a given refrigerant is assumed to have constant heat pumping potential per unit volume of material, then increasing the cycle frequency of a refrigerator using a fixed amount of the

refrigerant will subsequently increase its cooling rate. The device configuration affects this consideration in that the frequency of a device is not necessarily the cycle frequency of a given regenerator. The relationship between the machine frequency, f, and the cycle period, τ_C, is dependent on the magnet capacity factor and the number of high field regions:

$$f = (ab\tau_C)^{-1} \tag{79}$$

3.5.4.2. Utilization

The utilization parameter normalizes the quantity of thermal mass of the fluid displaced by the thermal mass of the refrigerant as defined by equation (47). Because specific heat of both the solid and fluid is variable with temperature, the utilization varies both spatially within the regenerator and temporally throughout the cycle. It is advantageous to use a reference value to specify a given ratio of thermal mass displaced to thermal mass of refrigerant:

$$\bar{\Phi} \equiv \frac{m_d c_f(T_\infty)}{m_s c_{ref}} \tag{80}$$

Where the specific heat capacity of the fluid is taken at the ambient value, T_∞, which is commonly room-temperature. For operating conditions outside of the room-temperature range, an average of the specific heat values found at the interface temperatures can also be used. The specific heat capacity of the solid is taken at a suitable reference point. For example, the phase transition value at the Curie temperature, T_{curie}, is sometime used.

3.5.4.3. Fluid Capacity Ratio

The frequency and utilization are operational variables which control the cooling power of an AMR device. A form of *capacity rate ratio* can be defined using these two parameters:

$$\dot{\varphi} = f\bar{\Phi} \tag{81}$$

This is essentially the rate at which the fluid thermal mass is displaced relative to the solid thermal mass. This term allows for cooling to be inspected as a function of a single control parameter rather than two.

3.6. Summary

Within this chapter, the principle elements related to the design and operation of magnetic refrigeration device are identified. Categories and classifications of these elements are defined. A framework for interpreting how these elements are assembled is presented. An approach and methodology to device design based on this framework is outlined.

In the following chapter, real magnetic refrigerators will be discussed. A newly constructed machine will be introduced. The design and development of this new device will be discussed in context of the knowledge accumulated from working with previously existing machines as well as referencing the design principles, framework and methodology suggested in this chapter.

Chapter 4: Machine Development and Apparatus

In this chapter, the experimental devices involved in this investigation are discussed. Two AMR refrigerator test apparatuses designed at UVic and have been used to produce extensive experimental data. Data from both of these machines are used in this study; therefore, their construction specifications and operational ranges are presented. A new machine has been constructed following based on the knowledge gained from working with the previous machines. The machine development is discussed with references to the principles of device design and framework outlined in Chapter 3.

4.1. Existing Devices

Two devices were previously constructed at the UVic and are still in operational condition. The first, built by Rowe [25], was intended to operate at either near-room or cryogenic temperatures. It employs a superconducting magnet with an axial-field orientation, is a D2 configuration with cylindrical regenerators, has a modulating flow style, and is a reciprocating type machine. The second, built by Tura [26], is strictly intended for near-room temperatures. It employs two dual nested Halbach arrays composed of permanent magnet material with a transverse-field orientation, is a D1 configuration with cylindrical regenerators, has a modulating flow style, and is a rotary type machine. Various other experimental and numerical results have been published regarding these machines [18] [20] [23] [24] [27] [28] [29] [30].

4.1.1. Superconducting Magnet Test Apparatus (SCMTA)

4.1.1.1. Device Specifications (SCMTA)

The test apparatus developed by Rowe employs a superconducting magnet to generate a constant axial magnetic field. Two active regenerators held at adjacent ends of a long cylindrical housing are reciprocated axially along the bore of the magnet such that the two regenerators are

in opposite magnetic phases (i.e. when one regenerator is magnetized in the high field region, the other is demagnetized in the low field region). This configuration is classified as D2 type. A rendering of the apparatus along with the regenerator housing is shown in Figure 14.

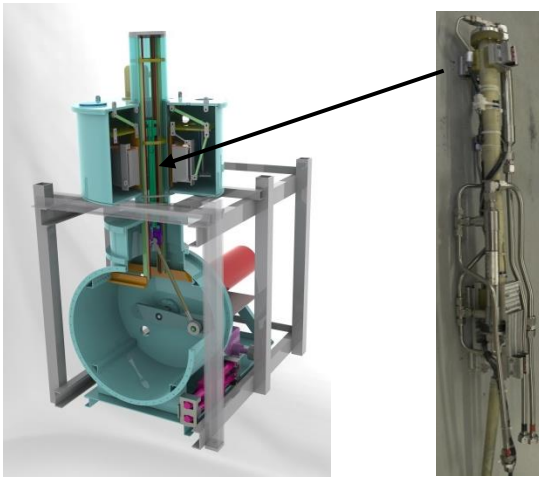

Figure 14: Rendering of SCMTA and photograph of the regenerator housing.

The motion of the regenerator housing is actuated by an electric motor which drives a piston-crank style mechanism. This produces a quasi-sinusoidal position waveform. Geometry, external forces, and inertial effects are the dominant causes for any variance in the waveform. The motion of the regenerator housing is mechanically coupled to a piston-cylinder fluid displacer mechanism. The HTF thereby oscillated in a modulating fashion across the regenerators in fixed phase with the magnetization cycle. Heat transfer fluids that are available for use include helium, nitrogen and carbon dioxide gases. Heat exchangers mounted on the regenerator housing maintain a constant heat rejection temperature. The regenerator housing including the heat exchangers and drive crank are held under vacuum to reduce ambient losses. Vacuum isolation is essential for cryogenic experimentation. A list of operating parameters and test variables are listed in Table 5.

Table 5: SCMTA machine parameters.

Heat Transfer Fluid	He, N, CO_2
Charge Pressure (P_0)	6.0 – 12.0 atm
Displaced Fluid Volume Range (V_D)	260 – 520 cm^3
Regenerator Volume Range (V_r)	13.0 – 52.0 cm^3
Machine Frequency (f)	0.5 – 1.0 Hz
Peak Magnetic Flux Density (B_H)	Variable, 0 to 5.0 T

4.1.1.2. Estimation of Thermal Losses (SCMTA)

The parasitic losses present in the SCMTA have been previously assessed [29]. The magnetic field vector in the SCMTA is applied axially with respect to the regenerator, therefore the demagnetization effects have been found to be small unlike transversal field alignment [30]. Also, because the system is held under vacuum, external convective losses are minimized. This reduces the significant parasitic heating mechanisms to eddy current generation and conductive heating through the support structure. Using a geometric model of the regenerator housing and support structure, the heat leak to the regenerator was numerically estimated to be linearly proportional to the temperature difference between the cold zone and the bearing support structure with an effective conductance loss coefficient of 0.16 W/K per regenerator. The overall expression for thermal losses to the device in the form of equation (53) is:

$$Q_L = 0.32(T_g - T_C) \tag{82}$$

where T_g is the temperature of the bearing support structure.

4.1.2. Permanent Magnet Test Apparatus (PMTA-1)

4.1.2.1. Device Specifications (PMTA-1)

The test apparatus developed by Tura [26] employs two assemblies of dual nested Halbach permanent magnet arrays to generate a variable transverse magnetic field. Two active regenerators in cylindrical housings are held stationary in the bore of the Halbach arrays. This

configuration is classified as D1 type. A rendering of the apparatus along with a cross-sectional view of the regenerator core within the magnetic field region is shown in Figure 15.

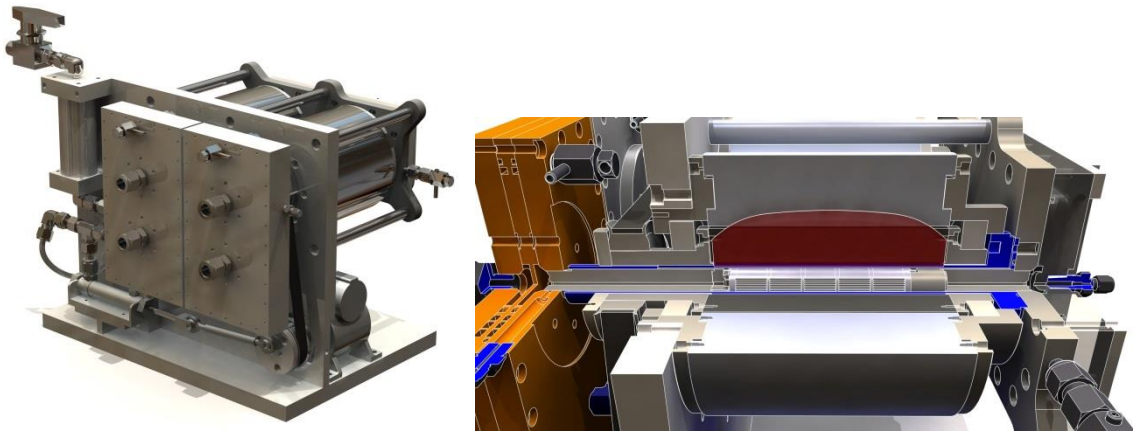

Figure 15: Rendering of PMTA-1 with cross-sectional view of the magnet and regenerator core.

The Halbach assemblies are constructed of eight wedge segments. Each segment has a fixed magnetic field vector such that when the segments are assembled in the Halbach, they combine to produce a uniform transverse magnetic field within the bore. The inner array rotates with respect to the stationary outer array. When the field vector within the bores of the two arrays are aligned the individual intensities of each array sum to the maximum high-field condition. When the inner array is rotated by 180° the fields cancel resulting in the minimum low-field condition. The two Halbach assemblies are 180° out of phase. This is explained graphically in Figure 16.

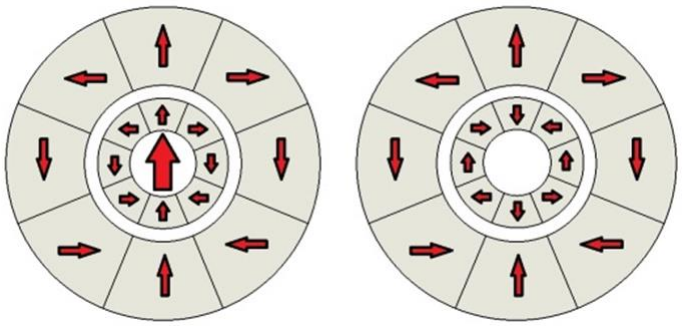

Figure 16: PMTA-1 Halbach field generators are shown in the respective high and low field conditions.

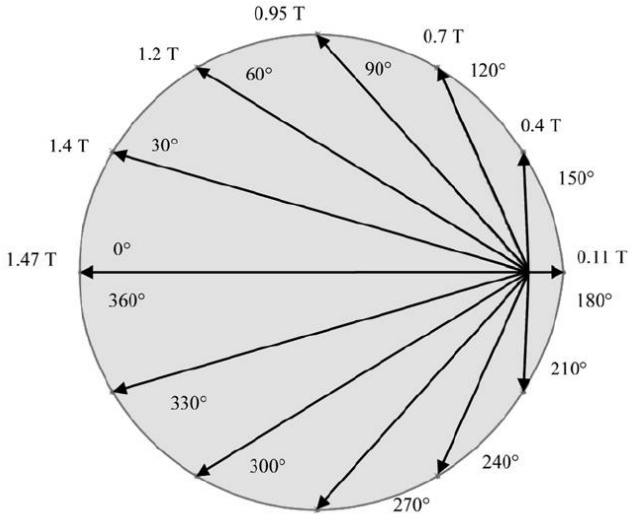

Figure 17: Graphical representation of the PMTA-1 field vector rotation within the Halbach bore [23].

Due to differences between the inner and outer arrays, the actual field strength at low-field is non-zero and the average strength of the low field over the half cycle is much higher than the minimum field. The field vector is aligned perpendicular to the regenerator axis. This contributes to increased demagnetization losses and resistive magnetic forces. This rotation of the magnetic field vector is represented graphically in Figure 17.

Table 6: PMTA-1 machine parameters.

Heat Transfer Fluid	H_2O + Glycol (80:20)
Charge Pressure (P_0)	4.0 – 6.0 atm
Displaced Fluid Volume Range (V_D)	2.5 – 10.0 cm^3
Regenerator Volume Range (V_r)	5.5 – 22.0 cm^3
Machine Frequency (f)	0.5 – 4.0 Hz
Peak Magnetic Flux Density (B_H)	1.47 T

The heat transfer fluid is liquid water with an ethylene glycol additive to prevent freezing. The heat transfer fluid displacement is mechanically coupled in fixed phase to the Halbach rotation. Stagnant fluid volumes exist between the regenerators and heat exchangers. Check valves on the cold heat exchanger mitigate this effect somewhat. Foam insulation is used

around the cold zone to reduce surface losses; however, the majority of the device is exposed. A list of operating parameters and test variables used with this device are listed in Table 6.

4.1.2.2. Estimation of Thermal Losses (PMTA-1)

The dominant losses for PMTA-1 are caused by convective losses to the surroundings. The environmental heat leak mainly occurs through the cold heat exchanger and through the regenerator shell. Because of the lack of metallic or thermally conductive components in proximity to the regenerator, the effects of eddy currents and direct conduction are considered negligible. A geometric model developed in *COMSOL* based on a regenerator geometry similar to regenerator #1 presented in Table 10 in chapter 5 was used to estimate the convective losses. The temperature was assumed to vary linearly across the regenerator. The simulation was run over a range of temperatures for these two components. The ambient temperature, T_∞, including the outer surfaces of the cold heat exchanger are defined as equivalent to the hot side temperature, T_H. The apparent heat leak was obtained by varying the cold zone temperature, T_C. The temperature along the inside of the regenerator was assumed to vary linearly from T_C to T_H. In order to simulate the rotating magnet, the outside boundary of the air was set to have a constant velocity based on the frequency of rotation. The thermal conductivity of each part was based on its material composition. Based on this model it was found that the heat leak was linearly proportional to the difference in temperature between the environment and the cold heat exchanger:

$$Q_L = 0.284(T_\infty - T_C) + 0.0297 \tag{83}$$

4.1.3. Knowledge Gained

The knowledge gained from operating these existing machines has highlighted some features to consider carefully when developing new devices. For instance, the Halbach magnet

approach, despite the imperfections of the field vector and waveform, is a compact method of producing a variable field while also eliminating the need for any dynamic sealing at the regenerator interface; this is a desirable feature. The fully modulating flow fashion works well in the case of the SCMTA where utilization is low, however with higher density HTF such as in the case of PMTA-1, stagnant fluid volumes result in measurable reduction of cooling; this is an undesirable feature. The beneficial or detrimental features of each machine are listed in Table 7.

Table 7: Comparison of the features of the SCMTA and PMTA-1.

	Advantages	Disadvantages
SCMTA	• Controllable field strength • High field strengths available • Capable of cryogenic temperatures • Static Sealing	• Limited to low machine frequency • Difficult to exchange regenerators • Low density gases difficult to seal • High magnetic forces • High power loss and parasitic heating due to friction
PMTA-1	• High machine frequency achievable • High utilizations achievable • Compact magnetic field generator • Low mechanical input power • All static sealing	• Non-stationary field vector • Unbalanced field waveform • Stagnant fluid volumes • Difficult to exchange regenerators • Limited refrigerant volume

Based on the experience with these two devices, a decision was made to maintain many of the features of PMTA-1 and try to address some of its shortcomings. With these considerations in mind, a new room-temperature permanent magnet refrigerator was designed and constructed.

4.2. Second Generation Permanent Magnet Test Apparatus (PMTA-2)

The second generation design is an extension of the original PRTA-1 device in that many of the basic features have remained the same [31] [32]. Both systems employ concentric nested

Halbach arrays to generate a variable magnetic field and are rotary style machines. The device is a D1 configuration. The regenerators are cylindrical and held stationary within the field region. Liquid heat transfer fluid oscillates through the regenerator by a piston-cylinder displacer in fixed phase with the magnetic cycle. This flow system is currently a hybrid style due to check valve control. A cross-sectional rendering and photograph of the new machine are shown in Figure 18.

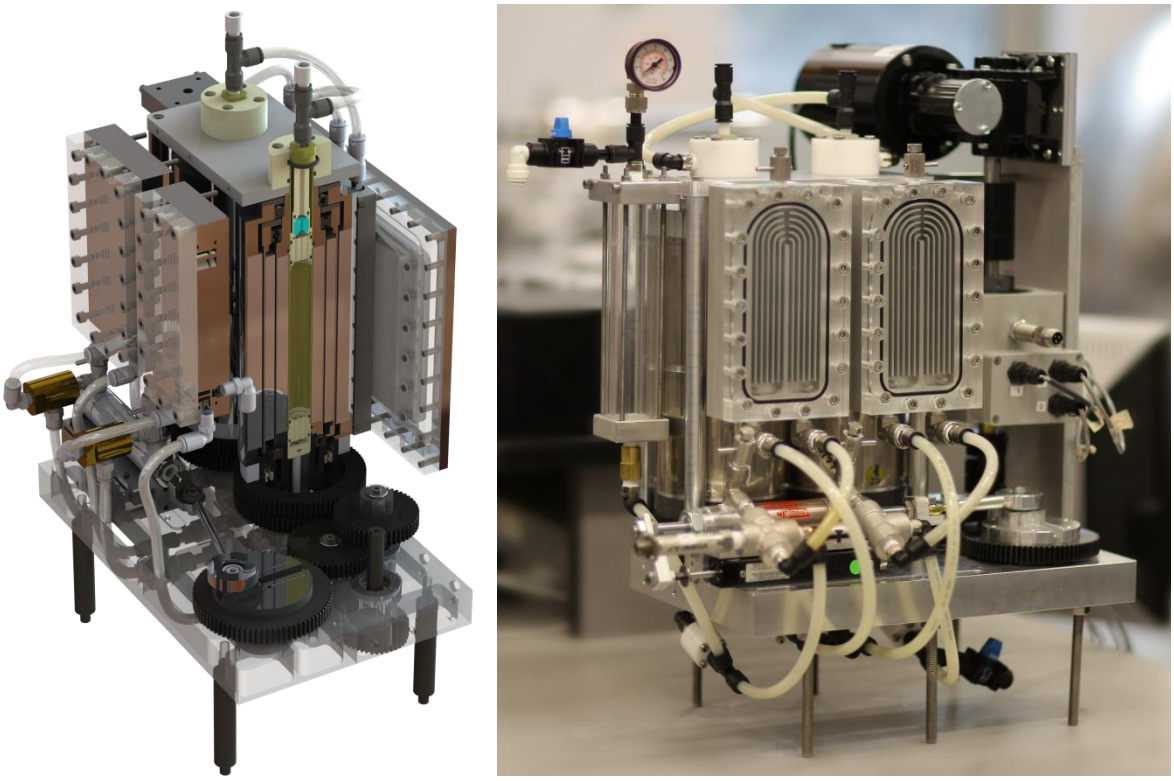

Figure 18: Rendering and a photograph of PMTA-2.

The most significant changes made with respect to the PMTA-1 device include the design of the magnetic field generators, the regenerator aspect ratio and the hydraulic system. Other features include a modular sub-system assembly and easily accessible regenerator core for fast material exchange. A list of operating parameters and test variables used with this device are listed in Table 8.

Table 8: PMTA-2 machine parameters.

Heat Transfer Fluid	H_2O + Glycol (80:20)
Charge Pressure (P_0)	4.0 – 6.0 atm
Displaced Fluid Volume Range (V_D)	2.5 – 10.0 cm^3
Regenerator Volume Range (V_r)	14.0 – 57.0 cm^3
Machine Frequency (f)	0.5 – 4.0 Hz
Peak Magnetic Flux Density (B_H)	1.54 T

4.2.1. Application

While the performance of the PMTA-1 in both temperature span and cooling power is appreciable, the system is limited in many regards. The best experimental no applied load temperature spans were in the range of 25-30 K and the best no-span cooling power is around 50 W using a total of 110 g of gadolinium spheres. The Risø group reported on a device providing cooling near 1 kW at zero span using 2800 g of gadolinium [10].

The new machine is intended primarily as a test apparatus; however, it is also expected to perform as a prototype refrigerator for common near-room-temperature cooling applications. The desired cooling power of the system is 175 W while operating between 0°C and 25°C. This implies that the no-span cooling power and the no-load temperature span must be on the order of 350 W and 50 K respectively.

4.2.2. MCM and Regenerator Design

Because this machine is intended to be an easily adjustable test apparatus, the exact nature of the regenerator (i.e. the MCM and morphology) is expected to change. Because Halbach magnets are used, the obvious choice of housing geometry is cylindrical; however, a square cross-section could also be installed if needed. Although there are no standards for assessing machine performance, gadolinium has become the benchmark refrigerant in near-room-temperature AMR research. To meet the cooling power requirement, the regenerator

housing would need to hold roughly seven times the amount of gadolinium spheres than could be installed in PMTA-1 at equivalent operational frequencies (i.e. 2 Hz).

4.2.3. Field Generator Design

The PMTA-2 field generator was designed to address some of the imperfections of the PMTA-1 design including the non-zero low field condition, rotating field vector and a non-sinusoidal waveform. The magnetic field generator was designed using *COMSOL* to predict the peak field states, field interaction between the Halbachs, and the magnetic field as a function of angular alignment.

The concept for achieving a balanced sinusoidal field waveform and a stationary field vector was to use three Halbachs rather than two. The purpose of this is to have the ability to rotate the intermediate and outer arrays in opposing directions with respect to a stationary inner array. The counter-rotating mode of a triple-nested Halbach assembly is shown in Figure 19. The inner array is stationary and produces approximately one half of the total high-field intensity. The intermediate and outer arrays each produce approximately one quarter of the high-field intensity. Analogous to the dual array design of PMTA-1, the three field vectors sum to full strength when their bore vectors are aligned and cancel when the intermediate and outer arrays are rotated 180° with respect to the inner array.

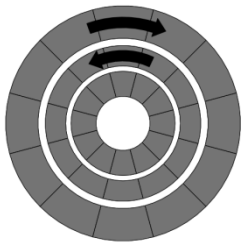

Figure 19: Triple array counter-rotating.

Simulations showed that this approach could be used to solve the magnetic field issues associated with PMTA-1. The simulated magnetic field waveform in the counter-rotating configuration for PMTA-2 is compared against the measured waveform of PMTA-1 in Figure 20.

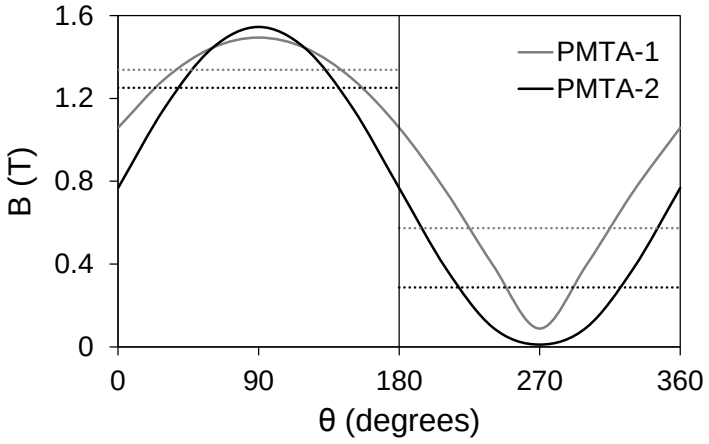

Figure 20: Magnetic waveform over one cycle, PMTA-1 measured, PMTA-2 simulated counter-rotating.

The dashed lines represent the mean flux densities, $\bar{B}_h$ and $\bar{B}_l$, of each machine for the respective half of the magnet cycle. Each of the three arrays is comprised of twelve magnet segments. Increasing the number of magnet segments improves the homogeneity of the magnetic field inside the bore. The field generator can also be operated in a co-rotating mode such that the intermediate and outer arrays rotate in the same direction. This mode produces essentially the same waveform as the magnet design in PMTA-1 which allows for more direct experimental comparison of the two magnet designs.

4.2.3.1. Magnet Utility Metric

The regenerator cross-sectional area and overall refrigerant volume were increased for PMTA-2. The benefits of this include lower pressure drop and higher cooling potential. The overall machine size is thus larger requiring greater amounts of both the permanent magnet and magnetocaloric materials; however, these materials are employed more effectively.

Because the inner magnet of PMTA-2 is stationary, more of the magnetic field volume can be filled with refrigerant due to no requirement for a clearance gap. To maximize the use of the high field region, the regenerator volume should be a large fraction of the field volume; however, this fraction will always be less than one due to the material housing and air gaps. The design parameters of the magnetic field generators, the useful field volume fractions as well as the comparative magnetic field utility, as defined by Equation (75), of the two different machines are presented in Table 9.

Table 9: Permanent magnet and refrigerant volume comparison for both machines.

Parameter	**PMTA-1**	**PMTA-2**
Total permanent magnetic material volume, V_{PM}	1250 cm^3	1500 cm^3
Permanent magnet volume per unit length of array	112 cm^3 cm^{-1}	75 cm^3 cm^{-1}
Total field region volume, V_B	41.8 cm^3	89.8 cm^3
Maximum possible regenerator volume, V_r	21.8 cm^3	69.7 cm^3
Fraction of field volume utilized, V_r/V_B	0.52	0.78
Mean high magnetic flux density, $\bar{B}_h$	1.34 T	1.25 T
Mean low magnetic flux density, $\bar{B}_l$	0.57 T	0.29 T
Difference in mean flux densities, $\bar{B}_h - \bar{B}_l$	0.77 T	0.96 T
Magnet utility, $\bar{\Lambda}$	12.32 mT	38.40 mT

4.2.4. HTF and Displacement System Design

The use of high density HTF was chosen. From the perspective of a test apparatus, water with a glycol additive is an attractive choice because it is a benign substance and easy to work with. The choice to use high density HTF leads to the thought that a continuous flow style is a more appropriate method; however, the use of a piston-cylinder displacer is mechanically convenient and there is less likelihood of the mechanism not functioning properly in terms of the AMR cycle. A hybrid alternative was developed as an intermediate step in the pursuit of a continuous flow system. The use of a piston-cylinder displacer could be maintained while at the

same time eliminating stagnant fluid volumes and improving heat exchanger effectiveness. In the future, a fully continuous flow system can be introduced without major modifications.

The hybrid method employs check valves with a very low cracking pressure (i.e. less than 4 kPa) adjacent to the regenerator and displacer. With the specific placement of the valves, the oscillating flow leaving the piston-cylinder is converted to unidirectional flow though the hot heat exchanger. The flow then returns to oscillating flow through the regenerator and is converted back to uni-directional flow through the cold heat exchanger. The check valves on the cold side of the regenerator are placed as close as possible to the regenerator interface to minimize stagnant fluid volume. The fluid leaving the regenerator during the cold blow is collected through the check valve and piped directly to the heat exchanger. This allows for the heat exchangers to be some distance away from the regenerator. The fluid re-entering the regenerator during the hot blow is exclusively fluid returning from the heat exchanger.

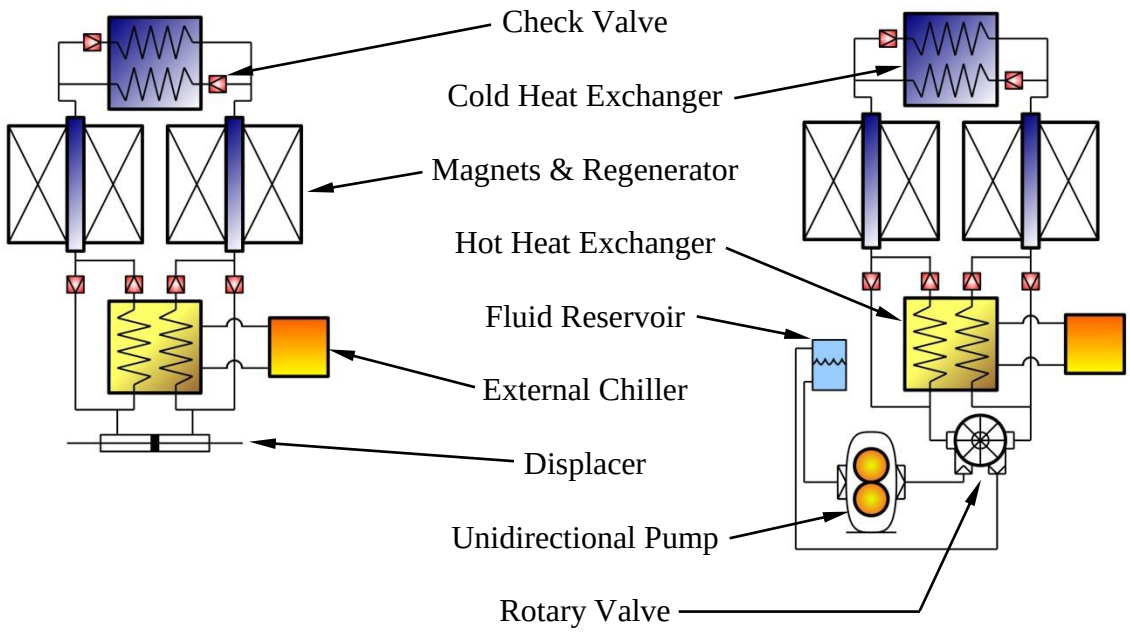

Figure 21: Fluid flow schematics comparing a double acting displacer arrangement to a unidirectional pump plus rotary valve arrangement.

A simplified flow schematic of the hybrid design is shown on the left side of Figure 21. The figure indicates a linked flow circuit where the two manget assemblies are 180 degrees of phase. Further, the displacer drives the HTF such that one regenerator is undergoing a cold blow while the other is undergoing a hot blow at the same instant. The displacer may be replaced by a pump and rotary valve mechanism to achieve a continuous flow system. The schematic for this case is presented on the right side of Figure 21.

4.2.5. General Considerations

PMTA-2 is primarily intended to be used as a test apparatus, therefore modularity, ease of use, and flexibility are some additional design objectives. To this end, the primary components are constructed independently. For example, the magnet assembly, displacer mount and gearbox are joined by their common base plates which can easily be moved or substituted. The regenerator section is also an independent component that is held in place by compression at opposite ends of the magnet assembly. The test section can be removed, materials or geometries exchanged and reassembled quickly. The hydraulic components outside the regenerator are connected by flexible nylon tubing with quick-push connectors. The capability also exists to mechanically couple a second system and cascade the regenerators or run them in parallel thereby doubling the cooling power. With the three available test machine introduced, the experimental portion of this investigation can now be presented.

Chapter 5: Experimental Data

This chapter presents all measurements and data collected pertaining to this investigation. Characterizing measurements are presented for PMTA-2 including magnetic waveform, magnet torques and system hydraulic losses. Data from a variety of experimental configurations and conditions using the three devices available at UVic are presented. The method of data collection is explained. The properties of the active regenerators as well as the operational conditions for all experiments are defined. The raw data is presented as the temperature span across the regenerator versus net cooling power. Some of this data is then presented in terms of exergetic cooling potential versus the net cooling power.

5.1. PMTA-2 Machine Measurements

5.1.1. Magnetic Field

The design of the PMTA-2 triple Halbach magnetic field generator intended to address problems with the PMTA-1 design. In particular, a balanced sinusoidal waveform with a fully zero low field state and a non-rotating field vector is desired. To measure the magnetic field an *Acquitek KOSHAVA5* Tesla meter is used. The single axis sensor is installed onto a measurement platform to control axial location along the bore and angular position about the rotational axis. The transverse field within the bore is measured. The sensor has a range ±2.0 T with an accuracy of ±0.01 T. Figure 22 presents the measured waveform data compared to what *COMSOL* simulations predicted. Figure 23 presents the axial field at high field and low field conditions.

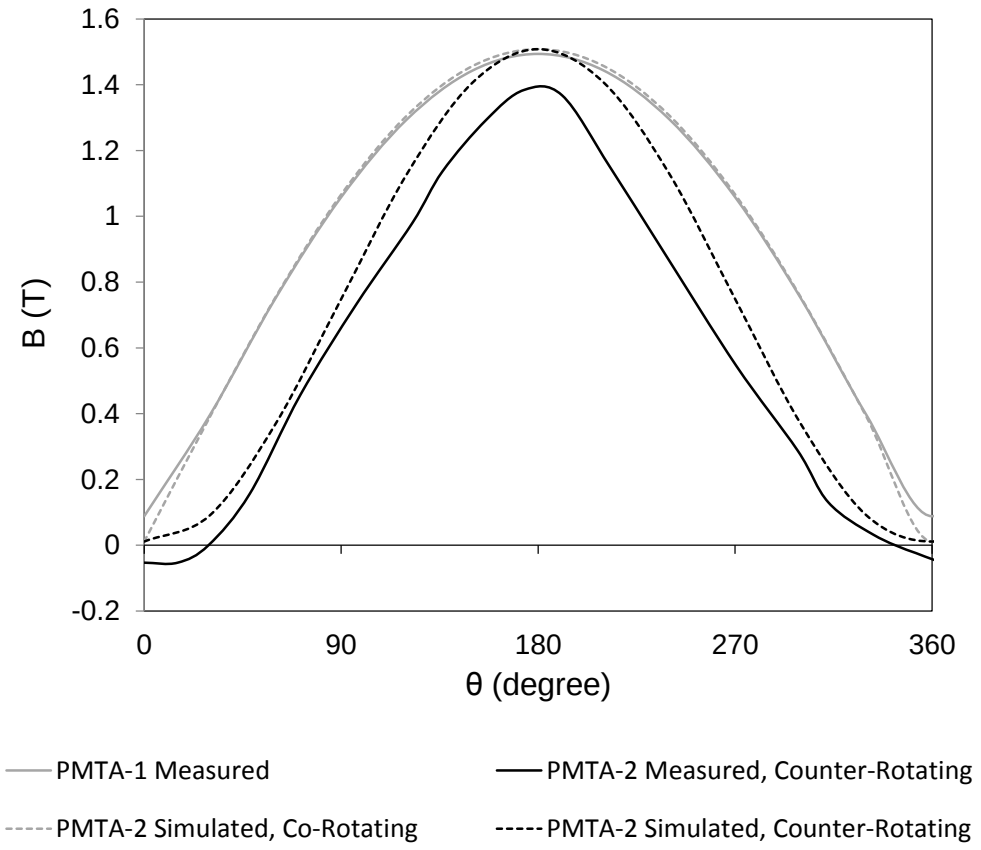

Figure 22: Simulated and measured magnetic field waveform of the PMTA-2 triple Halbach array.

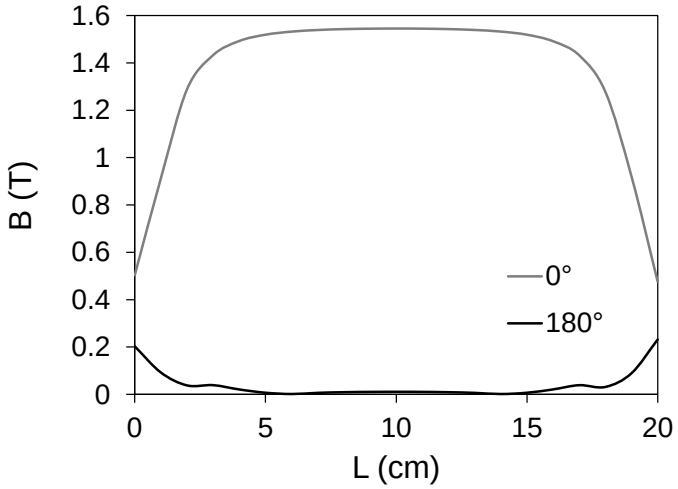

Figure 23: Measured magnetic field along the regenerator axis of the PMTA-2 triple Halbach array at 0 & 180 degrees.

5.1.2. Magnetic Torques

The torque observed to rotate the Halbach arrays dominates the mechanical portion of the power requirements to operate the device. The input torque required to rotate a single Halbach assembly in both the counter-rotating and co-rotating modes are measured. The torque required to rotate the intermediate and outer arrays in the counter-rotating mode was found to be significantly different than simulations predicted. Measurements are collected using a Himmelstein 48201V(1-2)-N-Z torque meter. The sensor has a range ±11.3 Nm with an accuracy of ±0.02 Nm. The measured torques are presented in Figure 24.

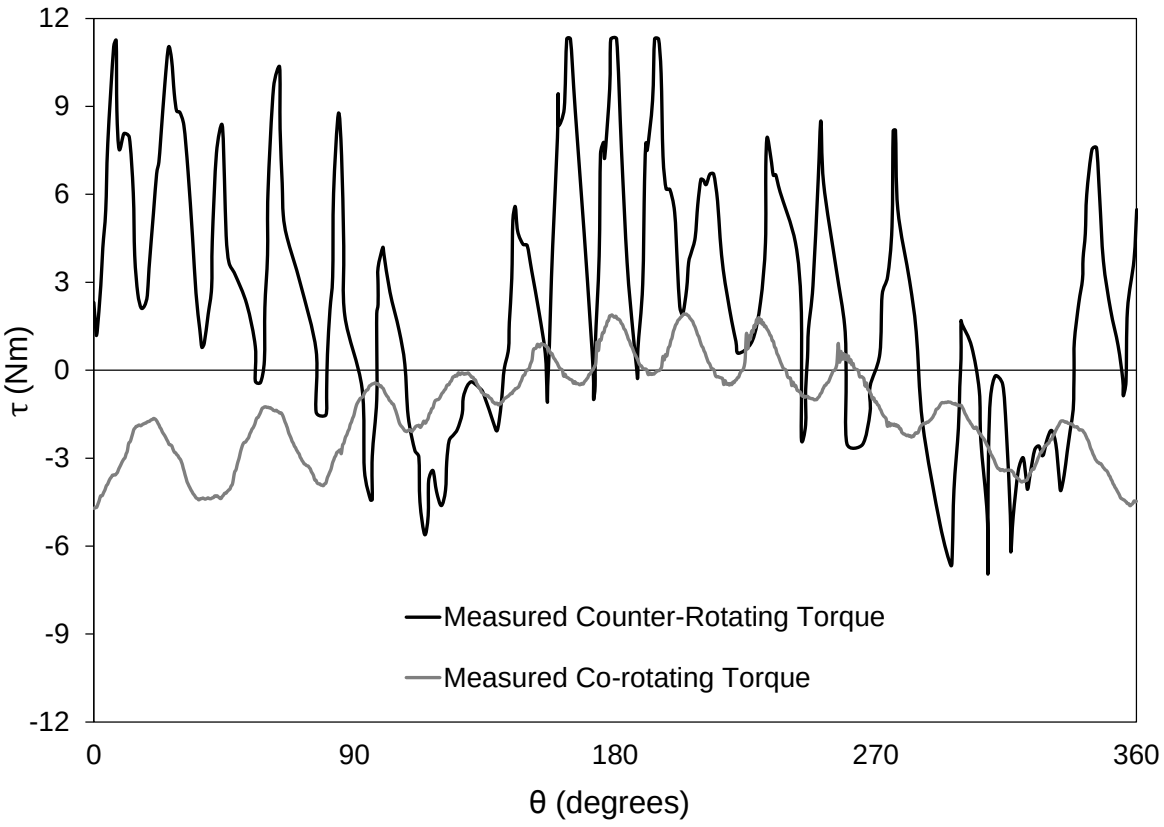

Figure 24: Measured counter-rotating and co-rotating torque waveform of one magnet array assembly.

Based on the measured torque waveforms and subsequent simulations, this problem is attributed to both manufacturing imperfections of the magnet segments as well as fringe field effects which are depicted in Figure 25.

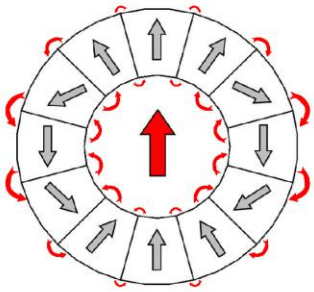

Figure 25: Representation of fringe fields of a Halbach cyclinder.

In an ideal Halbach cylinder, the flux through the bore is uniform and returns fully confined to the permanent magnet array. In practice, due to the finite number of segments, field uniformity inside the bore varies as the inner diameter is approached, particularly near the interfaces between two segments. Likewise, near the outer diameter, fringing fields are found near the ends of segments [33]. Because the PMTA-2 magnets are designed to have small spaces between the arrays, the interaction between fringing fields inside and outside of two neighbouring arrays is significant. The effects can be seen Figure 24 as a high frequency component in the torque waveform. As can also be seen, the torque waveform exhibits two quasi-sinusoidal oscillations per rotation; in other words, two torque cycles occur per one AMR cycle.

Because of this behaviour, setting two magnet assemblies 180° out of rotational phase does not result in the same torque reduction as in the PMTA-1 design, in fact, the opposite occurs where the torques sum to roughly double. Some solutions were examined including using four magnet arrays with the phasing in one pair adjusted to be 90° out of phase from the other pair. Even in this configuration, the net torque was too high to operate continuously. Because of this, the magnet assemblies have exclusively been operated in the co-rotating fashion where the intermediate and outer magnets rotate as one for all experiments. The torque requirement is significantly lower in this mode allowing for continuous operation; however, the magnet field

waveform is not the desired balanced sinusoid. It does still achieve a near zero low-field state in this mode. Some possible ways to reduce torque include leaving larger gaps between concentric Halbachs to reduce the interaction of fringing fields (as is the case in PMTA-1) or using more segments. End effects may also need to be addressed to reduce net torque.

5.1.3. Machine Pressure Drop

The pumping power is related to the viscous losses through the regenerator; however, the rest of the flow system also contributes to the net pressure drop. Pressure measurements are collected using *Omega* general purpose transducers with a maximum error of approximately ±10 kPa (±0.1 atm).

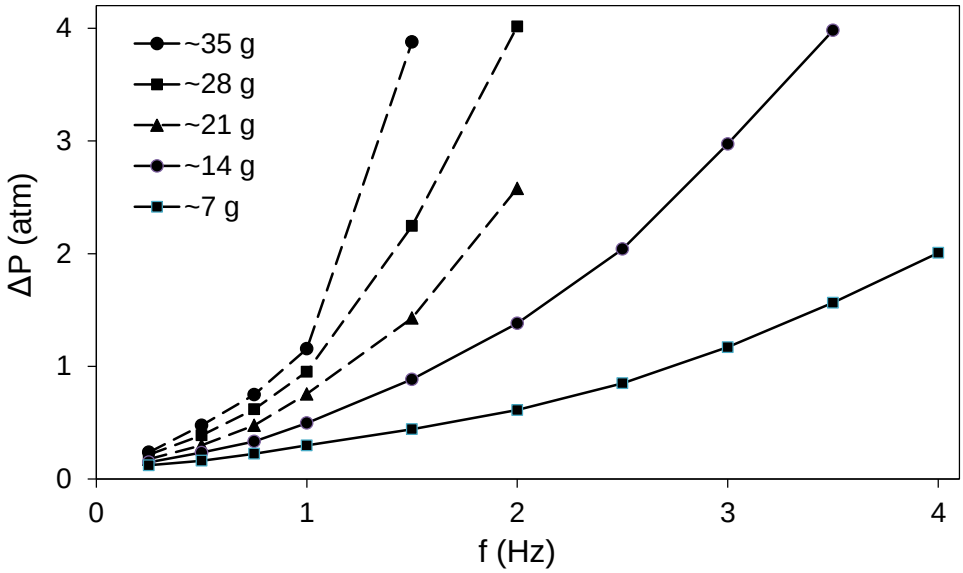

Figure 26: Hydraulic losses of the PMTA-2 machine without regenerators installed.

Figure 26 displays the pressure drop through the flow system without regenerators installed versus machine operating frequency at different displaced masses of water. It is evident that the flow system viscous losses are non-trivial especially at higher frequencies and displaced masses. With regenerators installed, the pressure drop across the regenerator itself can be extracted from net pressure drop measurements using this data.

5.2. Mechanical Power

Mechanical power, $\dot{W}_{mech}$, from Equation (64) describes the energy rate required to move the system including any friction and inertial forces. All three machines are driven by axial motors therefore measurements of input torques is known. The *baseline torque* is the measured torque required to operate the machine without a regenerator installed (i.e. independent of the AMR cycle of magnetic effects such as eddy currents) or fluid being displaced. The measured baseline torque of PMTA-2 is shown in Figure 27 along with measurements of PMTA-1 and SCMTA for comparison. These baseline torque values are always present and assumed to be constant regardless of operating conditions.

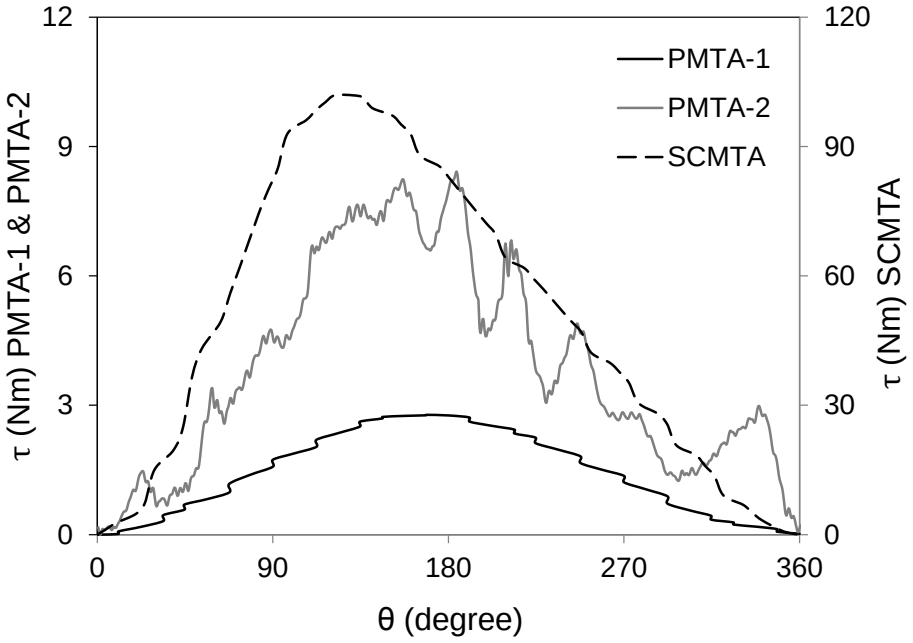

Figure 27: Measured torque requirements of all three devices (note that PMTA-2 field generators are measured in the co-rotating mode).

To calculate mechanical input power, torque is integrated over a full angular cycle and multiplied by the frequency. This calculation also assumes constant angular velocity.

$$\dot{W}_{mech} = f \int_0^{2\pi} \tau(\theta)\, d\theta \tag{84}$$

5.3. Experimental Method

Each of the three machines has a range of possible regenerator geometries as outlined in Chapter 4. Once regenerators are constructed and installed into the test apparatus and the HTF has been charged, experiments can commence. The heat rejection temperature is held constant by an external fluid temperature controller system. A known constant net cooling load is applied by means of an electric heater in the cold zone. Data is collected once the system achieves operational steady state, meaning the average cold zone temperature remains constant for an appreciable amount of time (i.e. 15 minutes). Measurements of temperature, pressure and torque are collected. This is done over a range of heat rejection temperatures and applied heat loads. Typical experimental data is presented in the fashion of temperature span across the regenerator versus the net applied cooling power. For tests using gadolinium, the temperature span versus net cooling power trend follows a nearly linear relationship.

5.3.1. Instrumentation

To measure temperatures in both permanent magnet machines, E-type thermocouple were used. These thermocouples have a rated accuracy of approximately ±1.0 K. In the case of the superconducting magnet machine, platinum resistance thermometers are used which have a slightly better accuracy of approximately ±0.5 K. Temperatures probes are located at the interfaces of both regenerators (i.e. two sensors on the hot-side and two on the cold-side). The average of the respective measurements is used to define the operating temperature span across the regenerators.

5.4. Experimental Conditions

5.4.1. Regenerators

In all cases, the refrigerant employed is gadolinium which is assembled into cylindrical regenerators either as spherical or crushed irregular particles. The features of each regenerator configuration are listed in Table 10.

Table 10: Regenerator properties of those tested in the SCMTA, PMTA-1, PMTA-2.

	Regenerator #1	Regenerator #2	Regenerator #3	Regenerator #4
Material Type	Gd	Gd	Gd	Gd
Curie Temperature (T_{curie})	295 K	295 K	295 K	295 K
Regenerator Geometry	Cylindrical	Cylindrical	Cylindrical	Cylindrical
Material Geometry	Spherical Particles	Spherical Particles	Irregular Particles	Spherical Particles
Effective Particle Size	~300 μm	~300 μm	~500 μm	~500 μm
Housing Diameter ($\emptyset$)	16 mm	25 mm	25 mm	22 mm
Housing Length (L)	55 mm	25 mm	25 mm	167 mm
Housing Volume (V_r)	11.1 cm^3	12.9 cm^3	12.9 cm^3	64.1cm^3
Refrigerant Mass per Regenerator (m_s)	55 g	65 g	45 g	325 g
Refrigerant Volume (V_s)	7.0 cm^3	8.2 cm^3	5.7 cm^3	41.1 cm^3
Porosity (α)	0.36	0.36	0.54	0.36
Number of Regenerators (r)	2	2	2	2
Total Mass (rm_S)	110 g	130 g	90 g	650 g

All of the PMTA-1 experiments are conducted with Regenerator #1. The same regenerator is also tested in the SCMTA. Regenerators #2 and #3 are tested exclusively in the SCMTA, while Regenerator #4 is tested exclusively in the PMTA-2.

5.4.2. Operating Parameters

Experimental data is collected on the four regenerators specified in Table 10 by the three machines. The experiments are labeled with a test number and the specific test conditions for each are summarized in Table 11. It is important to note that all of the experiments conducted with PMTA-2 employ the magnetic field generators in the co-rotating mode.

Table 11: Summary of all test conditions.

Test	Machine	R.	B_H(T)	HTF	P_0(atm)	V_D(cm^3)	f(Hz)	$\bar{\Phi}$(-)	T_H(K)
1	PMTA-1 2011	#1	1.47	H_2O	4	3.1	2.00	0.62	17, 22, 27
2		#1	1.47	H_2O	4	4.8	2.00	0.94	17, 22, 27
3		#1	1.47	H_2O	4	5.2	2.00	1.03	17, 22, 27
4		#1	1.47	H_2O	4	3.1	3.90	0.62	17, 22, 27
5		#1	1.47	H_2O	4	4.8	3.90	0.94	17, 22, 27
6		#1	1.47	H_2O	4	5.2	3.90	1.03	17, 22, 27
7	SCMTA 2011	#1	5	He	7	520	0.50	0.15	17, 22, 27
8		#1	5	He	7	520	0.75	0.15	17, 22, 27
9	SCMTA 2006	#2	1.5	He	9.5	520	0.65	0.12	15, 21, 31
10		#2	2	He	9.5	520	0.65	0.12	14, 21, 30
11		#3	2	He	9.5	520	0.65	0.12	15, 21, 31
12	PMTA-2 2012	#4	1.54	H_2O	4	10.5	0.50	0.36	20, 25
13		#4	1.54	H_2O	4	10.5	0.75	0.36	25
14		#4	1.54	H_2O	4	13.9	0.75	0.47	25

Note: Column "R." references the regenerator geometry from Table 10. Column "P_0" refers to charge pressure.

5.5. Experimental Results

5.5.1. Temperature Span and Cooling Power

This section presents the measured temperature span versus the net cooling power. All the data collected from experiment 1 through 14 are presented. There is too much data to present on a single plot therefore it was divided into four separate plots (a,b,c,d). The first (a) and second (b) plots show PMTA-1 results specifically experiments 1-3 at 2.00 Hz and 4-5 at 3.90 Hz respectively. The third (c) plot presents all the data pertaining to the SCMTA. The fourth (d) plot

presents all the data pertaining to the PMTA-2. The variation of the markers and line styles are identify the different experiment sets.

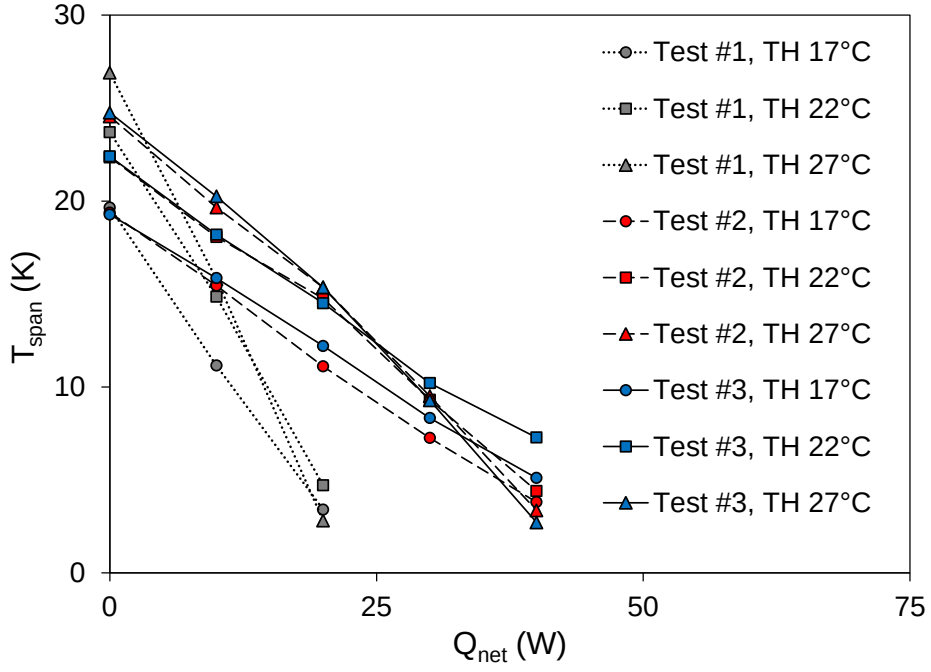

(a)

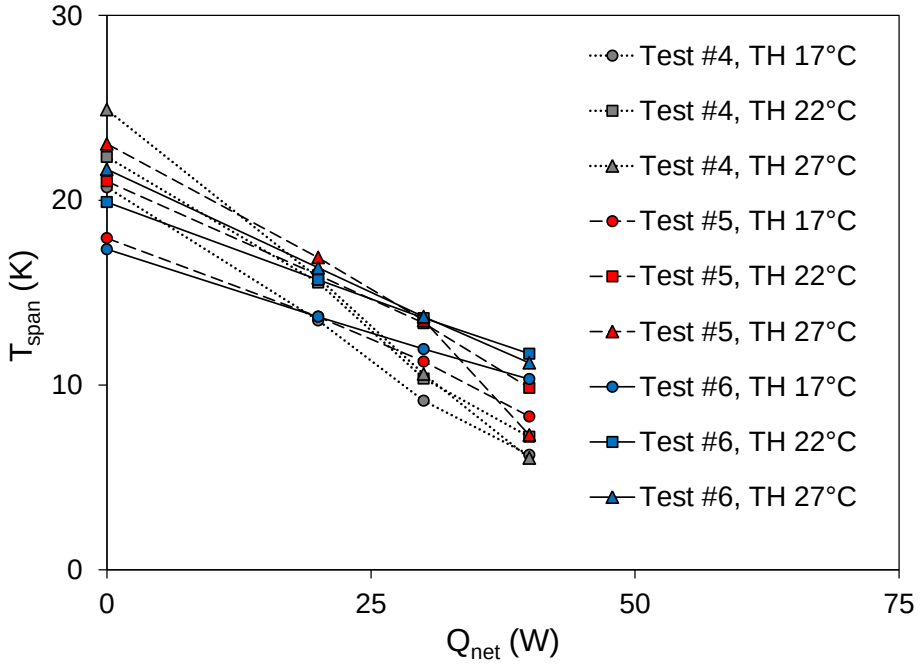

(b)

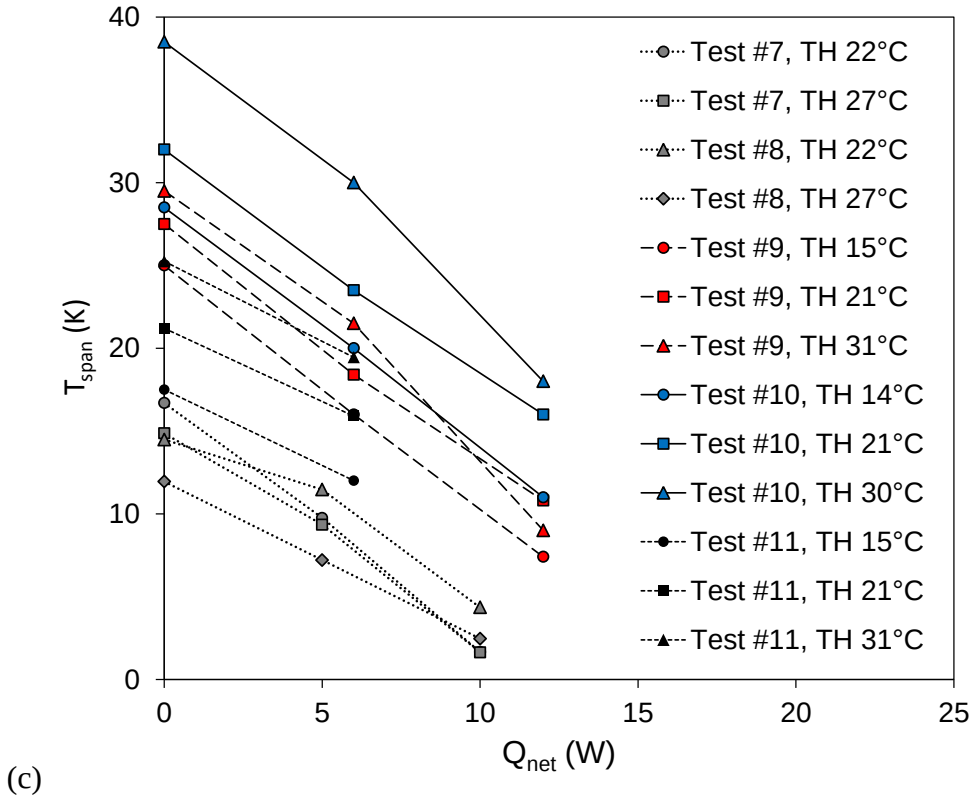

(c)

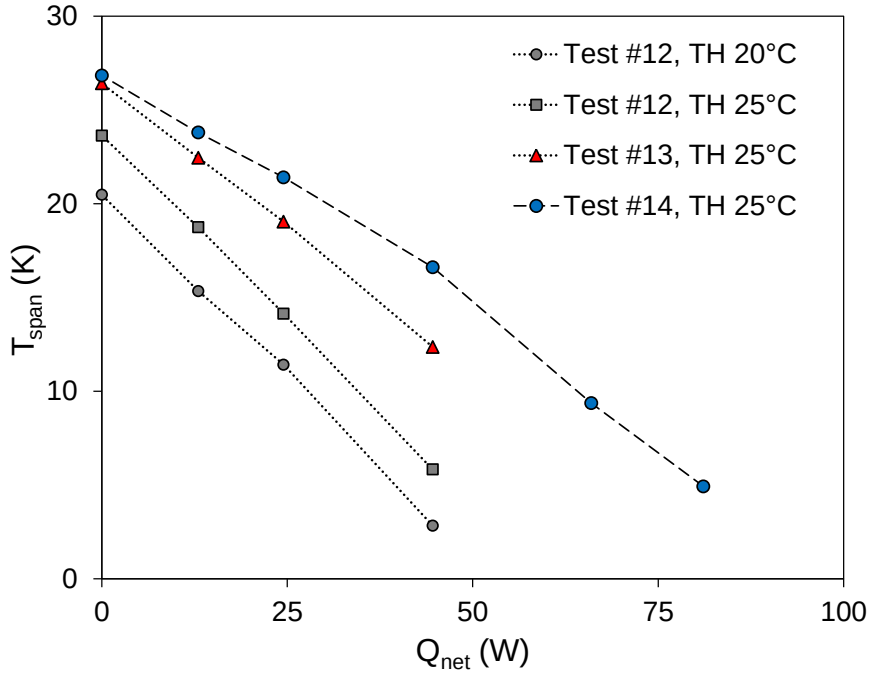

(d)

Figure 28: All SCMTA, PMTA-1 and PMTA-2 data presented as temperature span versus net cooling power. (a) shows tests 1-3, (b) shows tests 4-6, (c) shows tests 7-11, (d) shows tests 12-14.

5.5.2. Exergetic Cooling Potential

Useful cooling power can be more clearly shown using the exergetic equivalent as defined by Equation (68). The applied thermal load experimental results presented in Figure 28 is modified and presented again here in Figure 29 as the exergetic cooling potential versus net cooling power. Due to the quantity of data available, a representative selection from PMTA-1 is shown in the first (a) plot and all of the data from PMTA-2 is shown in the second (b). This selection of data will also be used in the analysis of Chapter 6.

In the case of the PMTA-1 data displayed in Figure 29(a), the maximum observed temperature span with zero net cooling is around 22 K and a maximum cooling power with zero span is estimated to be 96 W. This was seen in test #6. In terms of exergetic cooling power, the peak value is approximately 1.8 W corresponding to a net cooling power of 50 W with a 12 K span.

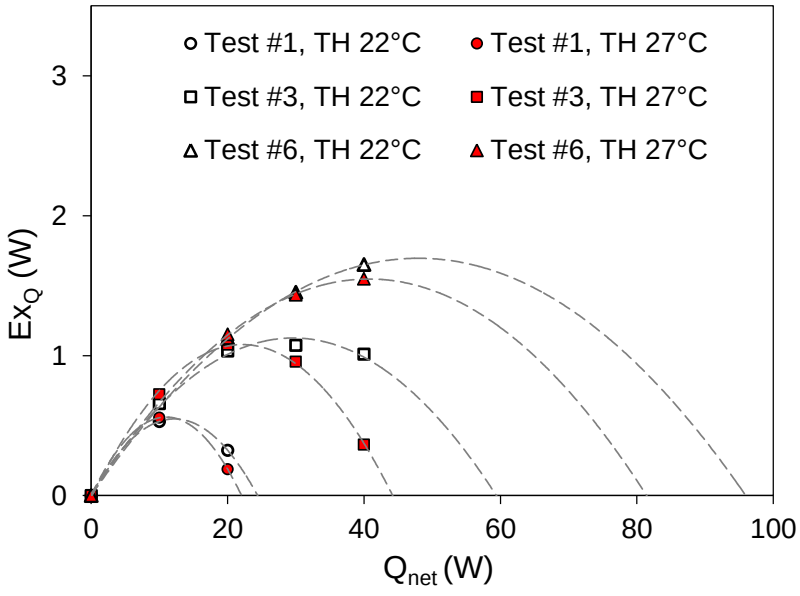

(a)

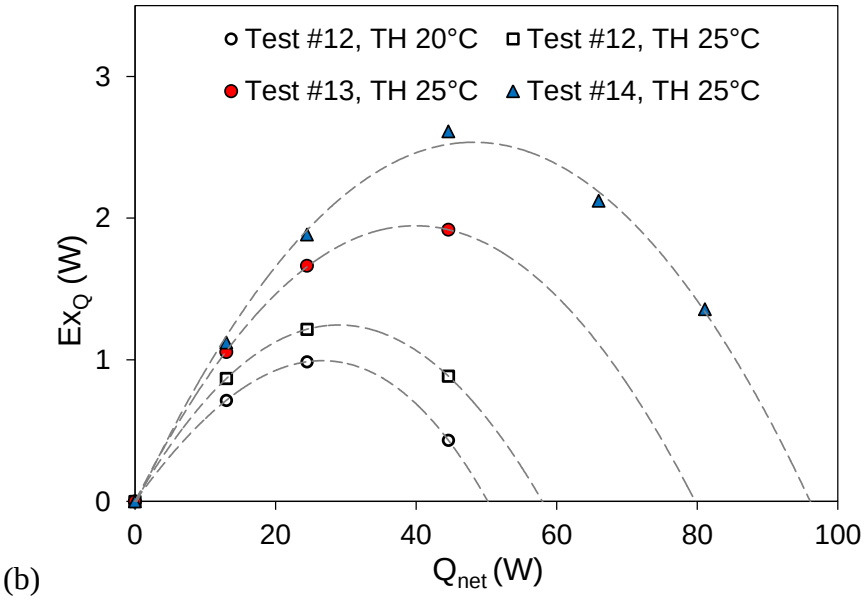

(b)

Figure 29: PMTA-1 (a) and PMTA-2 (b) results presented as exergetic cooling potential versus net cooling power.

In the case of PMTA-2 data displayed in Figure 29(b), the maximum observed temperature span with zero net cooling is approximately 33 K and a maximum cooling power with zero span is estimated to be 96 W. This was seen in test number 14. In terms of exergetic cooling power, the peak value is approximately 2.5 W corresponding to a net cooling power of 50 W with a 15 K span. The maximum power zero span condition was found from predictive parabolic curves displayed as dashed lines in Figure 29.

5.6. Summary

Presenting experimental data in the form of exergetic cooling potential versus net cooling power provides a means to determine the maximum useful cooling power of each device at different operating conditions. This is an improvement from the conventional temperature span versus net cooling power representations which only defines the limits of each service.

Neither of these representations of data adequately provides a basis for comparing the relative performance of two machines. The strength of magnetic field and amount of refrigerant

used has a dominant impact on results and must be considered in the comparison. For that, the specific exergetic cooling potential can be used. The FOM for the experiments can also be found to capture overall device performance. The method for identifying input irreversible work requirements is explained.

Chapter 6: Experimental Analysis and Discussion

The first half of this chapter analyses experimental data presented in Chapter 5 for PMTA-1 and PMTA-2, presents some comparable performance measurements and discusses the implications of those measurements. In the second half of this chapter, a hypothesis regarding the adiabatic temperature gradient is investigated. A semi-analytical relationship derived on the analytical expressions for cooling power is proposed.

6.1. Performance Analysis

The operational performance of the PMTA-1 and PMTA-2 are compared using specific exergetic cooling power and the second law FOM metric defined in Chapter 3. These metrics highlight desirable performance characteristics; namely, effective use of the refrigerant and magnetic field generator in the case of the specific exergetic cooling power and cycle efficiency in the case of FOM.

6.1.1. Specific Exergetic Cooling Potential

The specific exergetic cooling potential is determined by normalizing the exergetic cooling power by the product of volume of refrigerant and the average high field (Equation (73). In Figure 30, the specific exergetic cooling potential is plotted versus the net cooling power (a) as well as the fluid capacity rate ratio (b) which is defined by Equation (81). The open markers represent data from the PMTA-1 and the shaded markers represent data from PMTA-2.

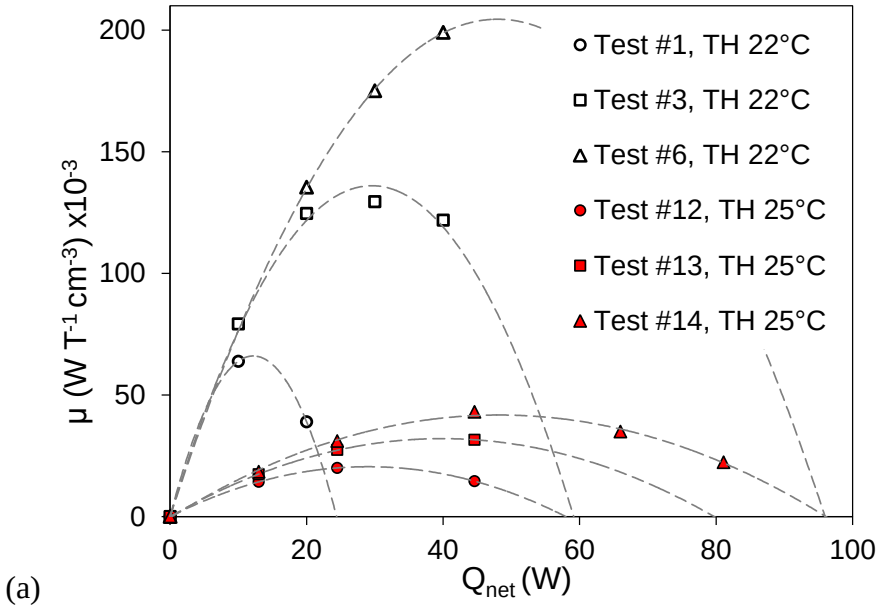

(a)

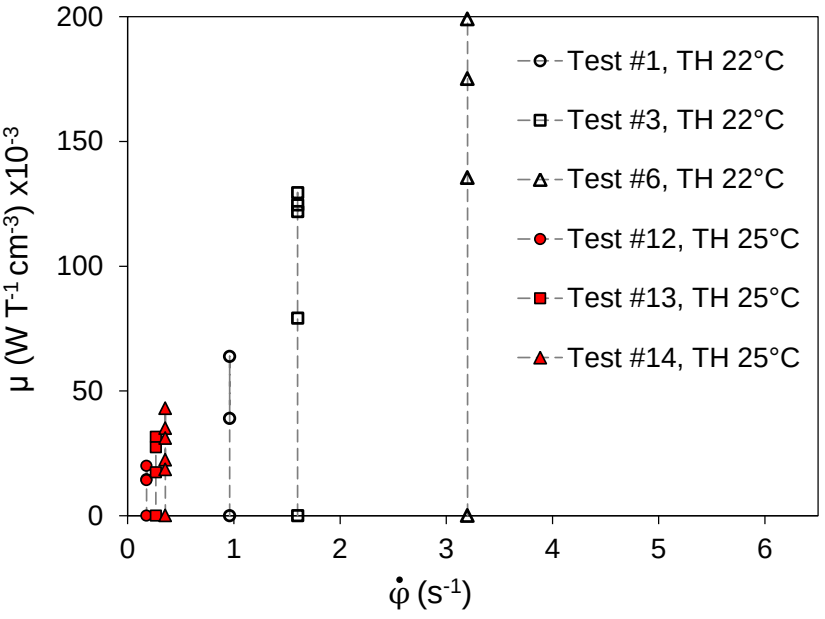

(b)

Figure 30: PMTA-1 and PMTA-2 results presented together as specific exergetic cooling potential versus net cooling power (a) and capacity rate (b).

The specific exergetic potential of PMTA-1 (tests #1, 3, and 6) is significantly higher than that of PMTA-2 (tests #12, 13, and 14) at equivalent net cooling. This implies that the refrigerant and magnetic field generator are employed more effectively to produce cooling. However, when

considering the fluid capacity rate ratio, PMTA-1 is also operated at a much higher range meaning there are subsequent input power requirements that drive efficiency down.

6.1.2. Figure of Merit

To calculate the second law efficiency FOM, the device work input must be accounted for. Recalling equations (71) and (72), the device FOM can be calculated from the exergetic cooling potential, $\dot{E}x_Q$, and the irreversible work rate input, $\dot{W}_{irr}$. The irreversible work rate is the sum of three elements: The pumping power, $\dot{W}_P$, the baseline mechanical power, $\dot{W}_{mech}$, and power loss associated with eddy currents, $\dot{W}_{eddy}$. The pumping power is a function of pressure drop (Equation (26) and is measured for all experimental cases. The baseline mechanical power of each machine is known and presented in section 5.2. For the case of PMTA-1 and PMTA-2, there are minimal metallic components in the vicinity of the magnets therefore it is assumed that eddy current losses are negligible.

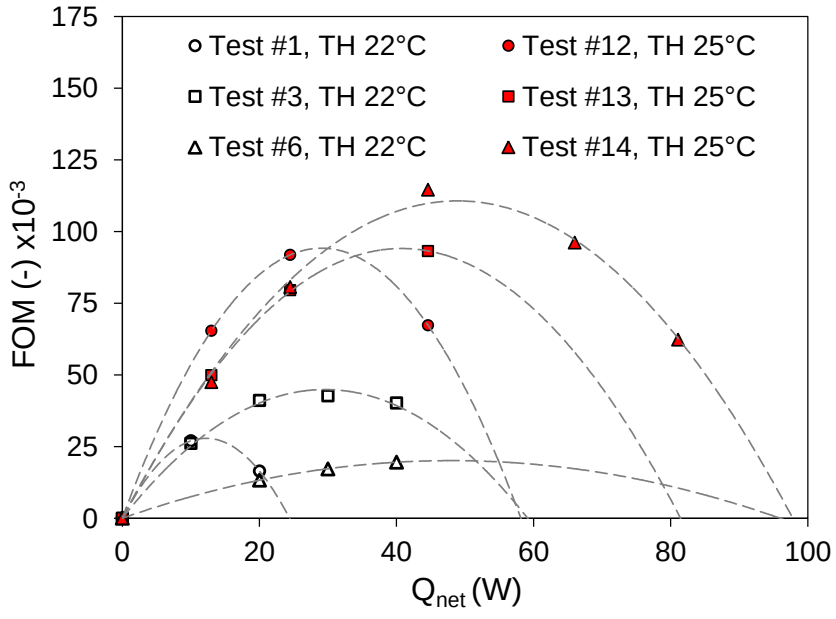

(a)

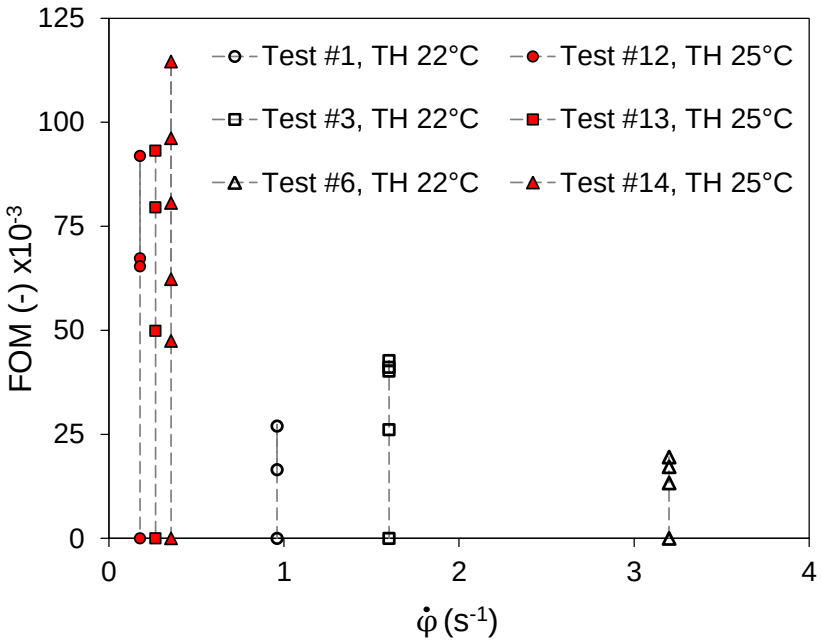

(b)

Figure 31: PMTA-1 and PMTA-2 results presented together as FOM versus net cooling power (a) and capacity rate (b) respectively.

Using the exergetic cooling data presented in Figure 29, pressure drop and fluid flow rate measurement for each experiment, and the baseline mechanical work of each machine, the FOM is calculated and presented in Figure 31 versus net cooling power (a) and capacity rate ratio (b). The FOM of PMTA-2 (tests #12, 13, and 14) is much higher than that of PMTA-1 (tests #1, 3, and 6) at equivalent net cooling. Similar quantities of service, namely cooling power and temperature, are delivered by both machines but the FOM results indicate that the PMTA-2 delivers these services more efficiently. The peak FOM observed for PMTA-2 is approximately 0.11. This is due to the high torques and pressure drop of the machine.

6.1.3. FOM versus $\bar{\mu}$

The results for FOM and specific exergetic cooling potential highlight different advantages of the two machines. PMTA-1 needs to operate at high capacity rates to achieve high cooling power which subsequently drives down efficiency; however, the cooling is achieved cost

effectively in terms of refrigerant and permanent magnet usage. PMTA-2 employs a large amount of material with bigger magnets meaning the cost effectiveness is low; however, the system is run at low capacity rates with high efficiency. One implication is that the maximum or no-span cooling power for PMTA-2 could be significantly improved by increasing capacity rate; however, this would negatively affect the FOM. Modeling suggests that PMTA-2 performance can be increased if the counter-rotating operating mode could be implemented; however, based on the results with the current magnets, this will likely require a new set to be manufactured.

By plotting FOM versus $\bar{\mu}$ in Figure 32, the divergent trends for these parameters can be seen. Ideally, both of these terms would be high, sending the trends to the top right corner of the plot. It is evident that capacity rate ratio has a strong impact on FOM.

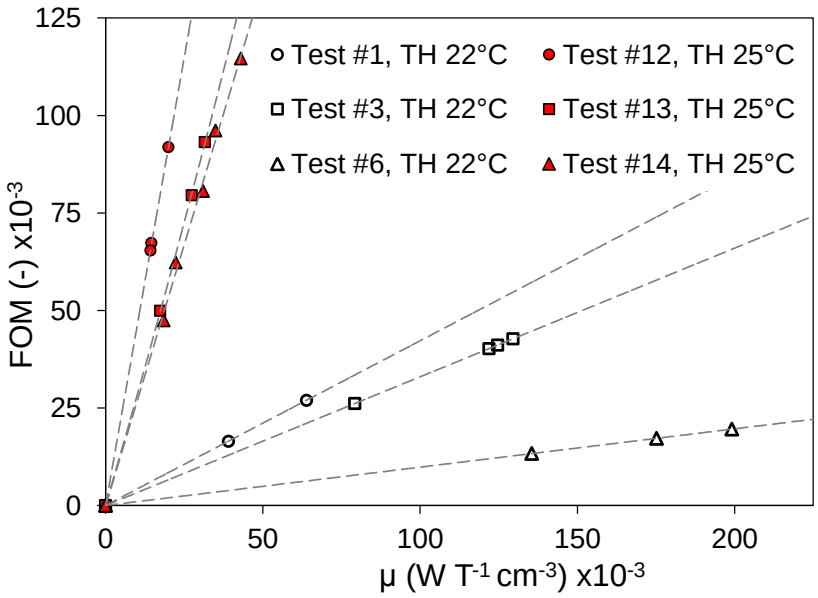

Figure 32: PMTA-1 and PMTA-2 results presented together as FOM versus specific exergetic cooling potential.

6.2. Semi-Analytical Relationship for Cooling Power

Due to the complexity of the fundamental AMR theory presented in Chapter 2, a desirable approach to designing AMR systems would be to use analytic expressions that describe

cycle performance through a direct calculation. Having such a tool would increase the rate at which the AMR parameter space could be mapped.

An analytic expression for cooling power based on the factors that determine AMR performance is defined by Equation (51). These factors include the refrigerant and fluid properties, effective conductivity, thermal mass ratio, cycle frequency, utilization, and reservoir temperatures. Based on numerous comparisons to experimental results, a modified form of Equation (51) is found to predict cooling power trends well using an effective MCE gradient [34],

$$\dot{Q}_C = \frac{m_s c_s}{\tau_c}\frac{\Phi}{R}\left(\frac{\Delta T}{T}\right)T_C\left[1-\left(\frac{\Phi}{2R}+\left(\frac{\Phi}{\kappa R}\frac{\Delta T}{T}\right)^{-1}\right)\left(\frac{T_H}{T_C}-1\right)\right] \tag{85}$$

All of the parameters but one, the effective adiabatic temperature gradient, can be described by a measured value, averaged value, reference value or linear relationship. The gradient is known to be different at every position within the regenerator and every instant in the cycle thus a single representative value is needed. In practice, the reservoir temperatures and net cooling power are measurable. The bulk cycle cooling is found from subtracting the thermal loss estimate for a given device from the net cooling. All other terms are specific to the experimental configuration and can be accounted for. This relationship is designated as semi-analytical because a single representative value for the gradient, which is a non-linear term, is taken from material data or experimental results and applied in an analytically derived expression. Reorganizing Equation (85) provides a semi-analytic expression for the gradient:

$$\left.\frac{\Delta T}{T}\right|_{S-A} \equiv \left[T_C-\frac{\Phi}{2R}(T_H-T_C)\right]^{-1}\left[\frac{Q_C\tau_c R}{m_s c_s \Phi}+\frac{\kappa R}{\Phi}(T_H-T_C)\right] \tag{86}$$

Because the reservoir temperatures are known, two values for the gradient can be calculated directly from MCE material data. Potentially, either of these values could be used in

the analytic expression of equation (85) to predict cooling power. As seen from the experimental finding in the following section, the minimum value of the adiabatic temperature change gradient calculated from each reservoir temperature can be used to estimate cooling power. i.e.:

$$\left.\frac{\Delta T}{T}\right|_{MCM} \equiv min\left[\frac{\Delta T_{ad}(T_H)}{T_H}, \frac{\Delta T_{ad}(T_C)}{T_C}\right] \tag{87}$$

6.2.1. Experimental Validation

The SCMTA and PMTA-1 were used to test three similar regenerators (#1-3) as outlined in Table 10. Tests numbers 1 through 11 were used as outlined in Table 11.

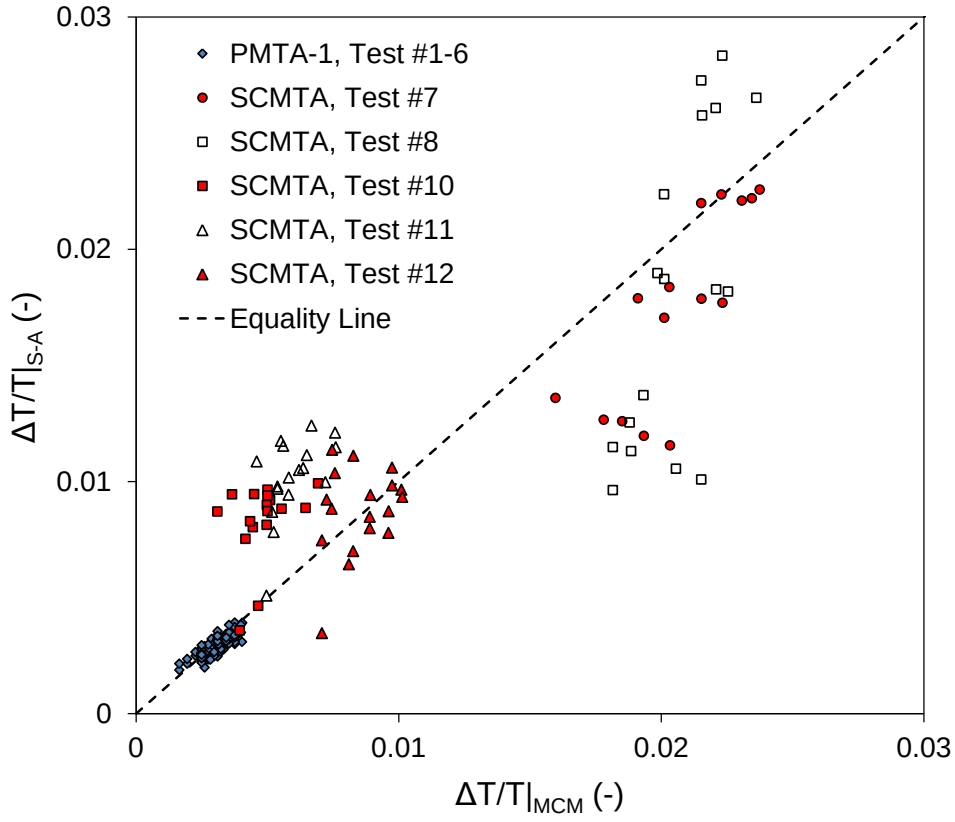

(a)

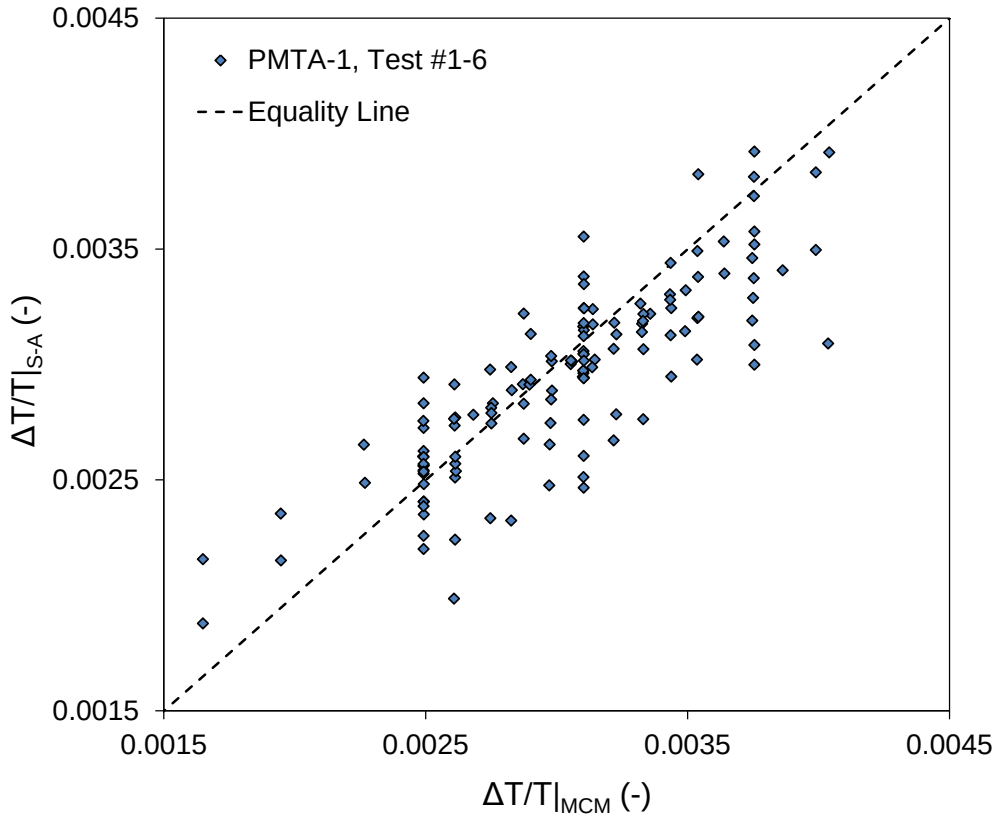

(b)

Figure 33: Values of the gradient calculated from the semi-analytical relationship and material data.

The experimental data is used to calculate separate values of $\frac{\Delta T}{T}$ from both the semi-analytical relationship of Equation (86) as well as the MCE data. The MCE curve for gadolinium presented in Figure 8 for is used to calculate $\frac{\Delta T}{T}$ at both the hot and cold interface temperatures and the minimum value is then taken as per Equation (87). The calculated values are plotted against one another in Figure 33. Points located near the diagonal equality line tend to satisfy the use of Equation (87) in the semi-analytical cooling power expression.

6.2.2. Comparison to Numerical Model

A previous AMR model was developed by Burdyny [18] which uses a single governing differential equation describing the temperature of both the fluid and solid. The impacts of imperfect convective heat transfer are accounted for by adjusting the effective thermal

conductivity term so that it appears within the regenerator energy balance equations. The method of combining conduction and convection into a singular effective thermal conductivity to predict AMR performance has shown good agreement with experimental results and other more complex numerical simulations. The MCE for the spheres used in the Burdyny model has been reduced by 25% of the measured value for pure Gd based upon modeling results compared to experimental results [27]. The Burdyny model is compared to predictions using the semi-analytical model.

Using the minimum gradient values taken from the MCE data of the refrigerant, the semi-analytical expression can be used to calculate the resultant cold zone temperature based on a fix hot reservoir temperature and a known cooling load. The semi-analytical model and the Burdyny model are compared against measured data from the PMTA-1. The results for the experimental conditions of test #3 in Table 11 are presented in Figure 34.

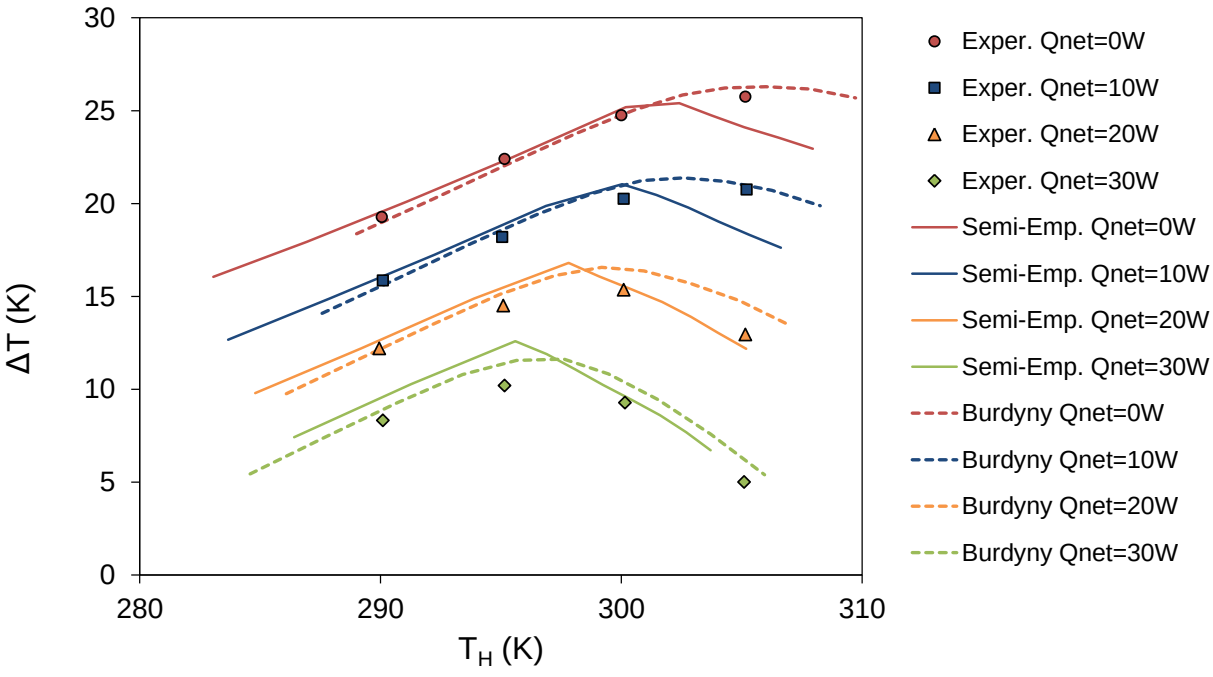

Figure 34: Experimental data compared against the semi-analytical model and Burdyny model for test #3.

The two models show strong agreement with the experimentally measured results from PMTA-1. The semi-analytical approach appears to achieve a reasonable level of accuracy while being less computationally intensive in comparison to the Burdyny model. The loss in accuracy is acceptable when computational speed allows for fast mapping of the parameter space. This method lends itself well to a first-pass design tool. The SCMTA results are poorly simulated by the semi-analytical method. The main reasons appear to be compressibility effects and pressure drop which are both significant. As pressure drop increases, the displaced mass decreases and the timing of the flow waveform is shifted with respect to the applied field waveform. A comprehensive comparison of the semi-analytic approach to experimental data for Gd spheres in PMTA-1 can be found in [34].

6.3. Summary

Two significant performance metrics were used to compare PMTA-1 and PMTA-2. Each metric gauges how well useful cooling is delivered and highlights different desirable characteristics: efficiency use of cost intensive components and efficient use of power to operate the system. PMTA-1 was found to operate with a higher $\bar{\mu}$ while PMTA-2 was found to perform with higher FOM.

A semi-analytical approach for defining an effective value for the adiabatic temperature change was discovered. Using this method, the cooling power can be estimated by a direct analytical calculation based on the reservoir temperatures. This approach was validated for the case of PMTA-1 against experimental data and a simplified numerical model.

Chapter 7: Conclusions

7.1. Summary

The objective of this thesis is to develop a framework for AMR device design. Such a framework is proposed that identifies and characterizes the primary system parameters, defines performance assessment metrics, outlines an approach to the design process and provides an analytical-based method for modeling AMR systems. There is no accepted method for conducting AMR device design. While this framework may not be the final solution, it is a feasible and concise approach for capturing the dominant factors and estimating performance for a given implementation. It also provides a basis for further development on how AMR device design can be best carried out.

The newest device at UVic, PMTA-2, highlights the value of a design framework due the variety of possible implementations of AMR devices. This device offers new insights into some machine construction methods and is compared to the existed devices at UVic. PMTA-2 is found to have better exergetic efficiency than PMTA-1 in part due to the low capacity rate ratio. This also indicates that increasing machine frequency could substantially boost cooling power as well as specific exergetic cooling power; however, the FOM will suffer as a result. Maximum observed temperature span with zero net cooling is around 33 K and a maximum cooling power with zero span is estimated to be 96 W. The maximum exergetic cooling power is approximately 2.5 W corresponding to a net cooling power of 50 W with a 15 K span. The peak FOM was observed at around 0.11. The absolute values of these figures may seem low; however, with such a wide range of device implementations and scales, the value of these normalizing metrics come from the meaningful performance comparisons between devices.

A semi-analytical relationship is developed and applied as a modelling tool. The semi-analytic approach is seen to predict experimental performance with similar accuracy as more complex numerical models.

7.2. Contributions

This thesis has contributed to the development of magnetic refrigeration technology in the following ways:

- A framework for design is proposed that specifies how the primary parameters of an AMR device impact operation performance. A methodology for processing through the design framework is also discussed.
- Existing metrics for ranking AMR device performance are collected and discussed in terms of applicability. The method for applying these metrics to experimental data is demonstrated and discussed.
- A new prototype refrigerator and test apparatus is presented. The design and construction are based on experience gained from previously existing machines and are discussed in terms of the dominant principles of AMR device design.
- Data from the new prototype device as well as data from other existing device is collected and analyzed. The performance is ranked using the metric defined here. A semi-analytic expression for cooling power was validated for use in the design process.

7.3. Recommendations

Good results were collected in this investigation but further work is recommended. The design framework is applicable in practice relating to the machines discussed in this thesis; however, it is necessary to compare results collect by other research institutions. The design space can also be mapped given the parameters outlined here.

The PMTA-2 machine still requires full characterization and some system improvements. Further attention to the magnet system could make a noticeable improvement to overall performance. By extension, managing the magnetic torques would allow for higher machine frequencies thus boosting cooling power. Extensive measurements of work consumption and cooling power over the control parameter space will show where the optimum operating condition is located. Examining different regenerator configurations is also advisable.

The semi-analytical relationship has shown good agreement with some experiments and poor agreement with others. It is clear that further validation is required. An appropriate first step is to compare a semi-analytical model of cooling power other existing numerical models. It also follows to validate the semi-analytical model against PMTA-2 results as well.

Bibliography

[1] Yu B., Liu M., Egolf P., Kitanovski A., 2010, A review of magnetic refrigerator and heat pump prototypes built before the year 2010, *International Journal of Refrigeration*, 33 (6), pg. 1029-1060.

[2] Nielsen K. K., Tusek J., Engelbrecht K., Schopfer S., Kitanovski A., Bahl C. R. H., Smith A., Pryds N., Poredos A., 2011, Review on numerical modeling of active magnetic regenerators for room temperature applications, *International Journal of Refrigeration*, 34(3), pg. 603-616.

[3] Smith A., 2013, Who discovered the magnetocaloric effect? Warburg, Weiss, and the connection between magnetism and heat, *The European Physical Journal H*, e2013-40001-9, pg. 1-11.

[4] Richard M.-A., Rowe A., Chahine R., 2004, Magnetic refrigeration: Single and multimaterial active magnetic regenerator experiments, *Journal of Applied Physics*, 95(4), pg. 2146-2150.

[5] Rowe A., 2012, Thermodynamics of active magnetic regenerators: Part I, *Cryogenics*, 52 (2-3), pg. 111-118.

[6] Gómez J. R., Garcia R. F., Carril J. C., Gómez M. R., 2013, A review of room temperature linear reciprocating magnetic refrigerators, *Renewable and Sustainable Energy Reviews*, 21, pg. 1-12.

[7] Smith A., Bahl C. R. H., Bjørk R., Engelbrecht K., Nielsen K. K., Pryds N., 2012, Material challenges for high performance magnetocaloric refrigeration devices, *Advanced Energy Materials*, 201200167, pg. 1-31.

[8] Bjørk R., Bahl C. R. H., Smith A., Pryds N., 2010, Review and comparison of magnet designs for magnetic refrigeration, *International Journal of Refrigeration*, 33, pg. 437-448.

[9] Rowe A., 2011, Configuration and performance analysis of magnetic refrigerators, *International Journal of Refrigeration*, 34(2011), pg. 168-177.

[10] Bahl C. R. H., Engelbrecht K., Eriksen D., Lozano J. A., Bjørk R., Geyti J., Nielsen K.K., Smith A., Pryds N., 2013, Development and experimental results from a 1 kW prototype AMR, *International Journal of Refrigeration*, DOI: http://dx.doi.org/10.1016/j.ijrefrig.2013.09.001.

[11] Callen H. B., 1985, Thermodynamics and an introduction to thermostatistics, *Wiley*, 2nd Edition.

[12] Engelbrecht K., Bahl C. R. H., 2010, Evaluating the effect of magnetocaloric properties of magnetic refrigeration performance, *Journal of Applied Physics*, 108, 123918.

[13] Basso V., Sasso C. P., Bertotti G., LoBue M., 2006, Effect of material hysteresis in magnetic refrigeration cycles, *International Journal of Refrigeration*, 29, pg. 1358-1365.

[14] Achenbach E., 1995, Heat and flow characteristics in packed beds, *Experimental Thermal and Fluid Science*, 10, pg. 17-27.

[15] Arnold D. S., Shopfer S., Tura A., Rowe A., 2009, Apparatus and method to determine convective heat transfer coefficient and friction factor in regenerators, *Third IIF-IIR International Conference on Magnetic Refrigeration at Room Temperature*, Des Moines, pg. 449-455.

[16] Ergun S., 1952, Fluid flow through packed column, *Chemical Engineering Progress*, 48, pg. 125-127.

[17] Vortmeyer D., Schaefer R. J., 1974, Equivalence of one- and two- phase models in packed beds: one dimensional theory. *Chemical Engineering Science*, 29, pg. 485-491.

[18] Burdyny T., Rowe A., 2013, Simplified modeling of active magnetic regenerators, *International Journal of Refrigeration*, 36, pg. 932–940.

[19] Rowe A., 2012, Thermodynamics of active magnetic regenerators: Part II, *Cryogenics*, 52 (2-3), pg. 119-128.

[20] Arnold D. S., Tura A., Rowe A., 2010, Experimental analysis of a two-material active magnetic regenerator, *International Journal of Refrigeration*, 34(1), pg. 178-191.

[21] Gschneider K. A., Pecharsky V. K., Malik S. K., 1996, The $(Dy_{1-x}Er_x)Al_2$ alloys as active magnetic regenerators for magnetic refrigeration, *Advances in Cryogenic Engineering*, vol. 42, pg. 475-483.

[22] Matsumoto K., Kondo T., Ikeda M., Numazawa T., 2010, Numerical analysis of active magnetic regenerators for hydrogen magnetic refrigeration between 20 and 77 K, *Cryogenics*, 51, pg. 353-357.

[23] Tura A., Nielsen K. K., Rowe A., 2012, Experimental and modeling results of a parallel plate-based active magnetic regenerator, *International Journal of Refrigeration*, 35(6), pg. 1518-1527.

[24] Rowe A., Tura, A., 2008, Active magnetic regenerator performance enhancement using passive magnetic materials, *Journal of Magnetism and Magnetic Materials*, 320, pg. 1356-1363.

[25] Rowe A., Barclay J., 2002, Design of an active magnetic regenerator test apparatus, *Advances in Cryogenic Engineering*, vol. 47 (613), pg. 995-1002.

[26] Tura A., Rowe A., 2011, Permanent magnet magnetic refrigerator design and experimental characterization, *International Journal of Refrigeration*, 34(3), pg. 628-639.

[27] Burdyny T., Ruebsaat-Trott A., Rowe A., 2013, Performance modeling of AMR refrigerators, *International Journal of Refrigeration*, DOI: http://dx.doi.org/10.1016/j.ijrefrig.2013.08.007.

[28] Rowe A., Tura, A., 2006, Experimental investigation of a three-material layered active magnetic regenerator, *International Journal of Refrigeration*, 29(8), pg. 1286-1293.

[29] Tura A., Roszmann J., Dikeos J., Rowe A., 2005, Cryogenic active magnetic regenerator test apparatus, *Advances in Cryogenic Engineering*, vol. 51, pg. 985-992.

[30] Peksoy O., Rowe A., 2005, Demagnetizing effects in active magnetic regenerators, *Journal of Magnetism and Magnetic Materials*, 288, pg. 424-432.

[31] Arnold D. S., Tura A., Ruebsaat-Trott A., Rowe A., 2013, Design improvements of a permanent magnet active magnetic refrigerator, *International Journal of Refrigeration*, DOI: http://dx.doi.org/10.1016/j.ijrefrig.2013.09.024.

[32] Arnold D. S., Tura A., Ruebsaat-Trott A., Rowe A., 2012, Design improvements of a permanent magnet active magnetic refrigerator, *Fifth IIF-IIR International Conference on Magnetic Refrigeration at Room Temperature*, Grenoble, pg. 309-315.

[33] Turek K., Liszkowski P., 2013, Magnetic field homogeneity perturbations in finite Halbach dipole magnets. *Journal of Magnetic Resonance*, DOI: http://dx.doi.org/10.1016/j.jmr.2013.10.026.

[34] Arnold D.S., Burdyny T., Rowe A., submitted 2013, AMR Thermodynamics: Semi-Analytic Modeling, *Cryogenics*, in press.